Sanati, S.; Abazari, R.; Albero-Sancho, J.; Morsali, A.; García Gómez, H.; Liang, Z.; Zou, R. (2021). Metal-Organic Framework Derived Bimetallic Materials for Electrochemical Energy Storage. Angewandte Chemie International Edition. 60(20):11048-11067. https://doi.org/10.1002/anie.202010093

# Metal-Organic Framework Derived Bimetallic Materials for Electrochemical Energy Storage

Soheila Sanati,[a] Reza Abazari,[a] Josep Albero,[b] Ali Morsali,[a]* Hermenegildo García,[b]* Zibin Liang,[c] and Ruqiang Zou[c]

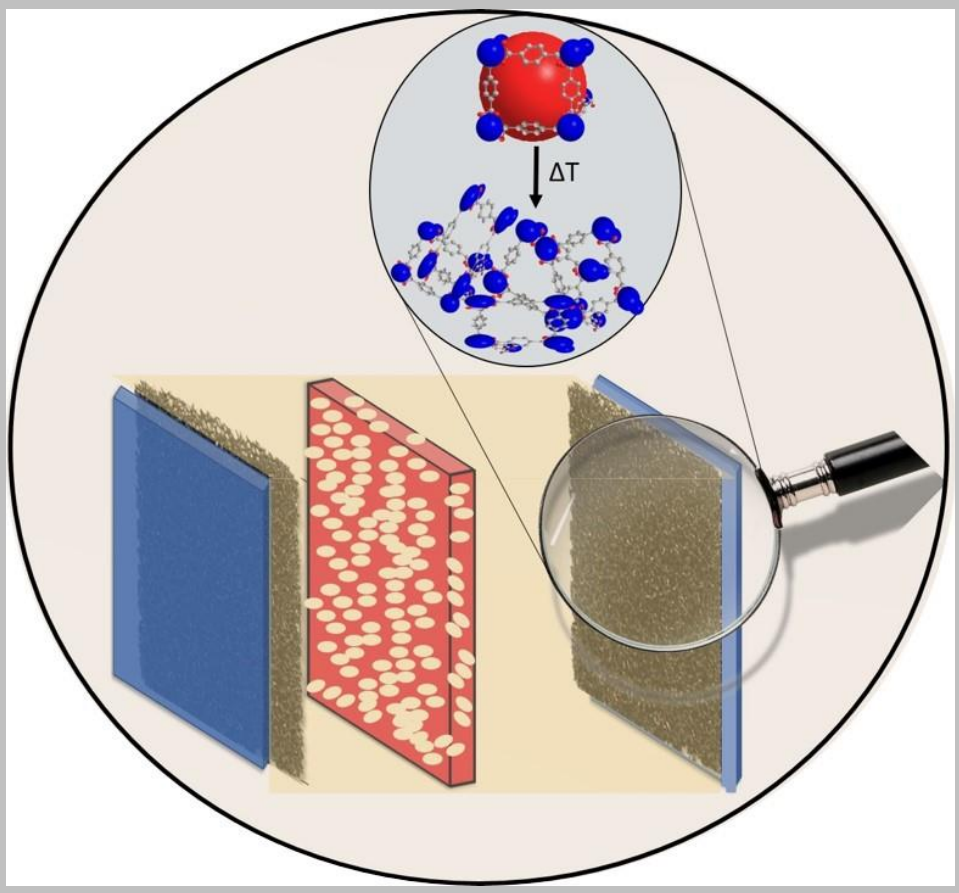


[a] Dr. Soheila Sanati, Dr. Reza Abazari, Prof. Ali Morsali
Department of Chemistry, Faculty of Basic Sciences
Tarbiat Modares University, Tehran, Iran, 14115-175
E-mail: morsali_a@modares.ac.ir

[b] Dr. Josep Albero, Prof. Hermenegildo García
Dep. De Química and Instituto Universitario de Tecnología Química (CSIC-UPV)
Universitat Politècnica de València, València, 46022 Spain
E-mail: hgarcia@qim.upv.es

[b] Dr. Zibin Liang, Prof. Ruqiang Zou
Beijing Key Lab of Theory and Technology for Advanced Battery Materials, Department of Materials Science and Engineering,
College of Engineering, Peking University, Beijing 100871, China

**Abstract:** Supercapacitors (SCs), showing excellent power density, long service life and high reversibility, have got extensive attention because of the increasing request for energy storage devices. To improve further their performance, it is essential to develop advanced electrode materials. A group of materials, which are porous crystalline solids, named metal-organic frameworks (MOFs) have proved to be excellent templates to synthesize functional materials to be employed in the preparation of electrodes for SC. In comparison to monometallic MOFs, bimetallic MOFs and their derivatives offer a series of advantages, including tunable electrochemical activity, high charge capacity, higher electrical conductivity. This review focuses on the use of MOF-derived bimetallic materials in SCs, paying special attention to understanding the origin of the improved performance and covering the latest developments in the field. Furthermore, the challenges and perspectives in this research area are discussed.

## 1. Introduction

The increasing energy demand and environment deterioration are crucial challenges in modern societies that have caused to quest for clean, abundant and renewable energy resources alternative to fossil fuels.[1] Solar and eolic energies have the capability to provide sufficient renewable electricity to cover most of the present and future energy demand. However, besides their intermittency, massive installation of renewable electricity based on solar and eolic energies has to be accompanied by affordable and reversible storage devices able to manage vast energy amounts.[2] Regarding electrical energy storage, increasing attention is being paid to SCs due to their high power densities, long operation life and short recharge times compared to dielectric capacitors and batteries.[3] Hence, SCs are considered among the key devices in the variety of the most promising energy storage systems.[4] SCs can be employed in heavy electric vehicles as well as portable electronic tools, and can complement batteries.[5]

SCs contain electrodes that are typically composed by active carbons (AC) with a large surface area, a separator to avoid short circuit, and an electrolyte (aqueous or organic electrolytes or ionic liquids) (see Scheme 1).[6] These devices store electrical energy at the interface between the electrode and the electrolytic solution, in a region termed as the electrical double-layer (EDL).[7]

Electrode materials are key components determining SCs efficiency. Besides carbons, a wide variety of electrode materials have been used in SCs fabrication, including MOFs, covalent organic frameworks (COFs), MXenes, metal oxides, metal chalcogenides, metal nitrides, layered double hydroxides (LDH) and black phosphorus, among others.[3b, 4, 8]

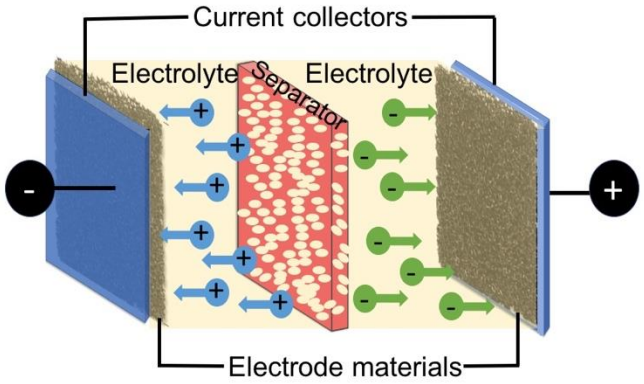


**Scheme 1.** Schematic illustration of a SC and its individual components.

One class of electrode materials are those in which the charge storage mechanism consists in the development of a EDL, without Faradaic reactions taking place. This category can be identified by recording rectangular cyclic voltammograms (CV), as well as by observation of a linear temporal dependence of potential at constant current. The charges are accumulated on the electrode surface under applied bias potential, while ions in the electrolyte are allocated in the electrode pores, resulting in a double charged layer at the electrode-electrolyte interphase. This type of SCs exhibit considerably more energy densities than the traditional capacitors due to the surface area increase and the decrease in distance between the electrodes. Furthermore, since the process of charge storage is ion migration instead of Faradaic redox reactions between the electrolyte and the electrodes, there are no chemical or compositional changes in the materials. This mechanism results in longer reversibility of consecutive charge-discharge cycles, increasing SC device operational lifetime over 500,000 cycles.

In a second category, the electrode materials show battery-like performance, and can be unambiguously distinguished from EDL by their Faradaic redox peaks in CV. The Faradaic reactions that govern the storage mechanism in this kind of devices shows peak-shaped current-potential responses proportional to the scan rate. Moreover, these electrodes are found in two different phases and compositions in the galvanostatic charge-discharge (GCD) diagrams.

Finally, a third category of electrode materials combines EDL and Faradaic reactions, forming a device known as pseudo-capacitors (PCs). The electrochemical features of PCs are neither purely capacitive nor Faradaic, involving Faradaic reactions and having, at the same time, a capacitive signature. Pseudocapacitance is obtained when surface-bond redox processes contribute to the total capacitance. This behavior is different from an ideal battery where, according to the Nerst equation, V is invariant with state-of-charge. The quasi-rectangular CV response resembles a capacitive EDL response, but in reality arises from a series of Faradaic redox couples with a potential distribution. That is, ideally, the redox peaks should overlay perfectly without any peak to peak separation. PCs can, therefore, be considered as a complementary form of EDCL since it is not a physical storage despite exhibits near-rectangular CV profiles and linear GCD curves similar to EDLC.[9] Scheme 2 summarizes the different types of electrode materials according to the charge storage mechanism.

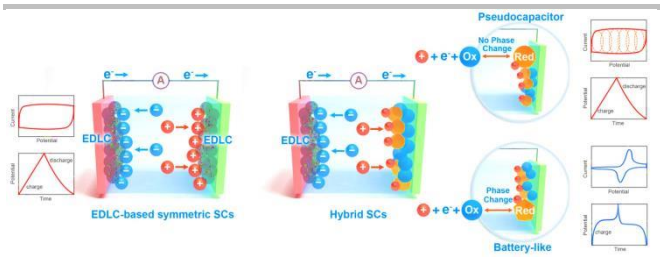


**Scheme 2.** Charge storage mechanism as EDLCs, PCs and battery-like electrodes.

It is also convenient to clarify the distinction between *hybrid* SCs and *asymmetric* SCs devices (ASDs). The term "*hybrid SC*" is used to indicate a device in which the two electrodes have different charge storage mechanism, meaning that one of them corresponds to EDLC and the other operates through Faradaic redox reactions. Accordingly, the resulting device is placed between an SC and a battery.[10] In contrast, ASDs correspond to a wide range of electrodes, including those SCs with the same electrode material, but different weight, and those others with different electrode materials. The reader should refer to existing comprehensive reviews for a deep coverage of the various SC types and their respective charge storage capacity.[3a, 11]

Pseudo-capacitance and EDLC are surface phenomena strongly associated with materials surface area and porosity. Accordingly, electrode materials exhibiting superior capacitance are those having large surface areas and suitable porous structures, increasing, therefore, the ion adsorption and diminishing transport distance.[12]

Ideal SC electrode materials have to demonstrate excellent electrical conductivity, high corrosion resistance, improved temperature stability, adjustable pore size, large surface area, and comparatively low cost. Typical nanostructured electrodes, including carbon-based materials,[13] transition metal oxides[14] or conducting polymers,[15] do not accomplish simultaneously all the above mentioned features, resulting in unsatisfactory capacitance, stability and/or production cost. Consequently, despite the considerable progress in the field, there is still plenty of room for a next generation electrode materials that can be prepared by means of ease scalable techniques, exhibiting high−performances and long-term stability.[16]

MOFs as a category of hybrid crystalline materials can form extremely porous materials with significant compositional and structural variations as they comprise coordinative bonds attaching multi-dentate organic linkers or ligands as well as transition metal ions or clusters (or secondary building units (SBUs)). The MOF organic linkers are normally organic carboxylates and organic multi-nitrogen compounds (like bipyridines, imidazoles, azoles, etc.), which correspond to the two major coordination modes namely oxygen coordination, and nitrogen-coordination. Scheme 3 indicates some instances of these SBUs and organic linkers as well as the relative MOFs. The large surface area and tunable pore size, along with the possibility to be modified after the synthesis and convenient upscaling production have attracted the interest of researchers in MOFs for a broad range of applications such as adsorption, sensing, catalysis, energy storage and drug delivery, among others.[18] MOF structural, electronic and chemical properties justify the massive current research effort that is likely to lead to various commercial applications.[19]

The application of MOF as electrode material is an emerging area that is quickly growing in two main directions.[20] On one hand, MOFs are used as templates or precursors to prepare carbons or porous metal oxides that often inherit adjustable micropore size (i.e., 0.6-2.0 nm) and high surface areas.[21] On the other hand, MOFs can integrate electrochemical redox centers and, in this way, they can be used directly as electrode material.[22]

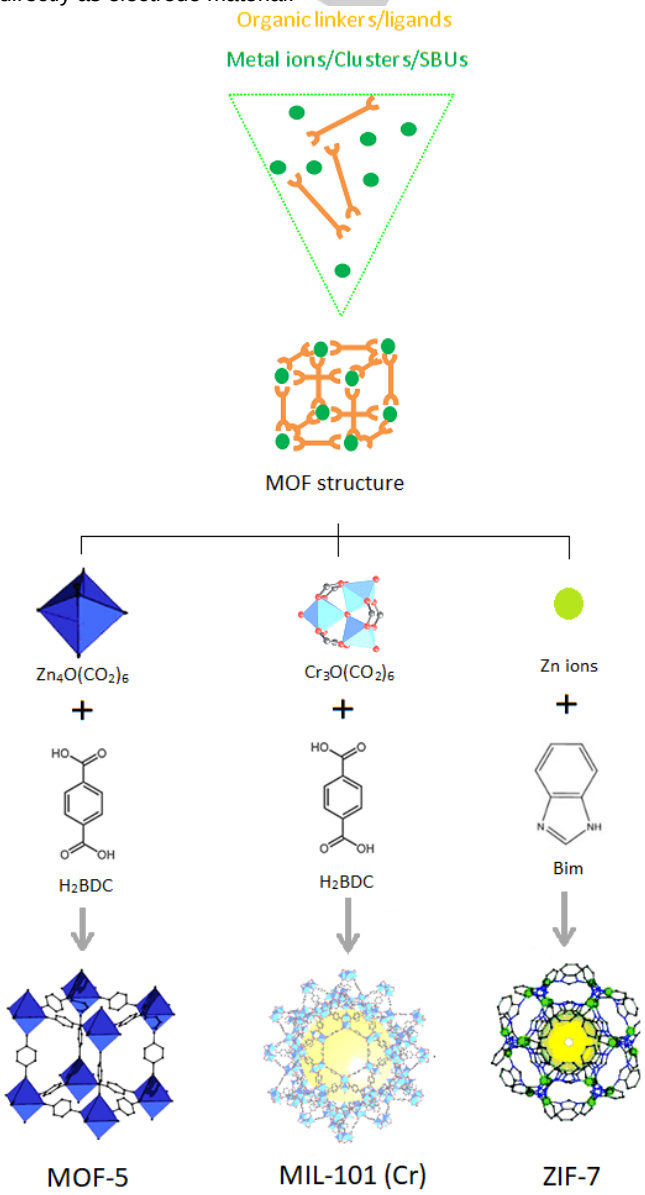


Scheme 3. Examples of some MOF structures.

The use of MOFs as sacrificial templates to obtain derived carbons, metal oxides or the combination of both offers the advantage that several key properties of MOFs determine the structure of the resulting derived material. Particularly noteworthy, the flexible design of MOFs makes them customizable and versatile templates,[23] and a uniform porosity of the resulting material is often the result of the MOF crystal structure. Conversion of the organic MOF components into carbon materials through carbonization/pyrolysis without additional external carbon sources in a single step is another advantage of using MOFs as templates/precursors of electrode

materials.[24] On the other hand, it is possible to remove the organic ligands from the template/precursor MOFs during the thermal treatment leading to the derived material leaving the metal clusters that can be converted into metal oxides, metal sulfides or other small nanoparticles. Materials produced through these approaches are promising, environmentally benign and cost-effective solutions for energy storage.[25]

Besides precursors, there are also a few reports on the direct use of MOFs as SC electrodes, taking advantage of the flexible structure they can offer.[26] For instance, a Co-MOF has shown a capacitance of about 2474 F $g^{-1}$ at a current density of 1 A $g^{-1}$.[27] However, the low electrical conductivity and steric hindrance to ion insertion are still serious limitations to be overcome for the direct application of MOFs as SC electrodes. Structural stability is an additional issue, since there is, in general, a lack of MOF stability in the presence of the typical electrolyte solutions employed in SCs.[28, 29] The flexibility in the design of tailored MOFs should open, however, in the future the possibility to overcome these limitations.[30] An improved charge transfer inside the framework might be achieved by the adjustment of linker size and structure; in addition, redox reactions could be facilitated by using MOFs with metal cations exhibiting low redox potentials.[31] In this context, it is clear that development of MOFs exhibiting easy electron migration would be a milestone in the area. Besides, MOFs with adequately large pore size or void volume are also convenient to allow fast electrolyte diffusion.[22, 32] Furthermore, MOF metal cations can be selected using the approach named “matched electrolyte solution” to implement the material with the capability to store charges via an electrochemical reaction, thus, increasing the total capacitance.[33 A very promising approach in this regard is the design of bimetallic MOFs.[22]

Bimetallic MOFs are a new kind of MOFs that have attracted considerable interest in recent years.[34] Bimetallic MOFs can sometimes be prepared by modifying the synthetic procedure of a given MOF adding certain amounts of a second metal ion. Frequently, the reaction between a ligand with two metal ions of similar charge density and electronic configuration gives rise to mixed-metal bimetallic MOFs as a single phase rather than a combination of two monometallic MOFs. Bimetallic MOFs, like monometallic MOFs, have been employed as electrode materials in different fields following the two previously commented strategies. Thus, bimetallic MOFs are applied either directly as electrode materials or as template/precursors in the preparation of advanced materials, such as mixed metal phosphides, mixed metal oxides, mixed metal hydroxides, mixed metal selenides and mixed metal sulfides, or as composites based on bimetallic MOFs (Scheme 4). To be specific, pristine bimetallic-MOFs containing the electrochemical activated sites like the metal nodes and organic linkers can be utilized for the redox-involved electrochemical applications. Moreover, the cations, ions, as well as protons placed in the pores or on the surfaces of MOFs allow this type of materials to serve as a new generation of conducting media. While various bimetallic MOF materials have been investigated before, they have some disadvantages when used as supercapacitor electrodes, including poor electrical conductivity, capacitance retention, and/or cycling stability. Consequently, developing a bimetallic MOF-derived material with good rate efficiency, great capacitance retention, and superior cycling stability for supercapacitor applications is extremely demanded. Also, compared to MOF-derived monometallic materials, analogous bimetallic derivative products can offer advantages of more diverse and efficient electrochemical activity, higher electrical conductivity and stability, among others.

Among the different applications of materials derived from bimetallic MOFs, their use as electrode materials in SCs has experienced a considerable interest in the recent years. The existing reviews, however, do not describe in detail most of the recent research articles in this area.[35] These recent studies have shown that materials derived from bimetallic MOFs exhibit a superior performance compared to the analogous ones obtained from monometallic-MOFs.

Given that most of the reports of MOF-derived bimetallic materials are very recent, the field of bimetallic materials and derivatives applied to energy storage materials has not been yet revised. The present review is intended to fill the gap, providing the reasons behind the improved performance of MOF derived bimetallic materials as electrodes for SCs. After presenting briefly the latest advances in the field of MOF−derived materials for SC application, the following sections provide an extensive review of the reports on MOF-derived bimetallic materials, indicating the different material types, their preparation methods and reasons behind the superior performance in SC devices.

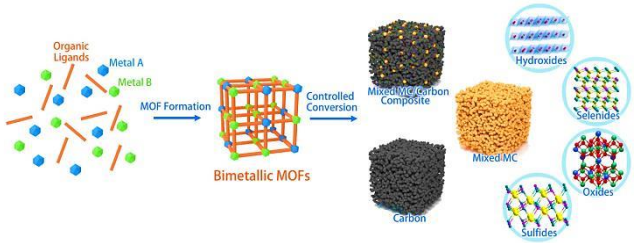


**Scheme 4.** Schematic illustration of different structures derived from bimetallic MOFs.

## 2. Recent advances in MOF derived materials

The two main parameters influencing capacitance of materials are surface area and porosity.[36] MOFs are among the materials with the highest specific surface area, often in the range of 1000−6000 $m^2$ $g^{-1}$.[37] Moreover, since MOFs may possess a broad variety of redox centers, they could, in principle, be used directly as electrode materials. However, steric hindrance to ion insertion due to pore dimensions, incompatibility of some MOFs with electrolytes and lack of electrical conductivity are the main challenges yet to be overcome for the direct use of MOFs in SCs.[38]

While the direct use of MOFs in SCs has still to break several limitations, a large number of studies have appeared in recent years showing the advantages of MOF−derived materials in electrical energy storage.[33b-e] The overall outcome of this extensive research is the improved performance and stability of MOF−derived materials, particularly over the direct use of MOFs, with the real possibility that these materials become commercialized in electrical storage energy devices. The best studied types of MOF-derived materials achieving high performance SC electrodes are carbons, metal chalcogenides, hydroxides, oxides and their hybrid composites.[39]

Conductive carbons are the most widely used materials in SCs. Many different types of carbon materials such as carbon nanowires/nanotubes, porous carbons, graphene and

derivatives, among others, have attracted considerable attention as electrode materials for SCs, because of their abundant and renewable sources, good chemical and thermal stability and affordable costs.[40] Some of these carbon materials can be obtained by MOF carbonization under inert atmosphere. For instance, Qian *et al*. found out that micro/mesoporous carbon materials are reliably formed from a robust cage-based zinc organic framework (named BMM-9) as precursor upon pyrolysis under inert atmosphere at high temperatures.[41] This carbonaceous residue showed laminar structure (Figure 1 a), large surface area, stability and efficiency as SC electrode. The GCD outcomes for BMM-9-T (T meaning the treatment temperature) materials demonstrated that at a current density of 1 A $g^{-1}$, the specific capacitance corresponding to BMM-9-900 (182.8 F $g^{-1}$) is higher than the specific capacitances corresponding to BMM-9-1000 and BMM-9-800, which are equal to 141.7 $Fg^{-1}$ and 140.0 $Fg^{-1}$, respectively (Figure 1 b).[41] The different capacitance values measured correlate with the structural parameters (pore size and surface area) in the carbon materials formed at each temperature, which affect ion transport. The cycling stability of BMM-9-900 was remarkable, maintaining 98.5% of the primary capacitance (132 F $g^{-1}$) at the current density of 10 A $g^{-1}$ following $10^3$ cycles (Figure 1 c). These values indicate an excellent cycling electrochemical stability that derives from its structural and chemical stability in 3 M KOH solution.[41]

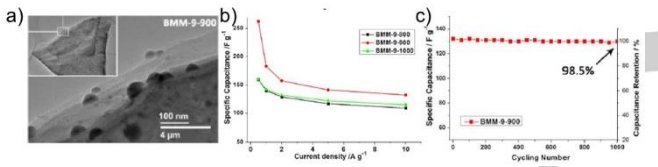


**Figure 1.** (a) TEM image of BMM-9-900 (scale bar 100 nm). Inset shows a general view of the carbonaceous particle at large magnification (scale bar 4 μm). (b) Specific capacitance retention as a function of discharging rate from 0.5 to 10 A $g^{-1}$ for BMM-9-800 (black), BMM-9-900 (red) and BMM-9-1000 (green). (c) Cycling stability performance of BMM-9-900 obtained from discharging rate at 10 A $g^{-1}$ for 1000 cycles. Reproduced with permission from Ref.[41] Copyright 2018, the American Chemical Society.

Metal oxide nanostructures for electrical energy storage in SCs have attracted particular attention due to their surface area, shape, size, and porosity. Several physical and chemical methods proposed for metal oxide preparation lack reliability, even at laboratory scale, due to the influence of experimental parameters in the resulting material. In contrast, MOFs can be reliably and efficiently converted to metal oxides upon calcination. The typically observed pore size in the MOF-derived metal oxides, together with their high specific surface area make them good SC materials. In this regard, Maiti et al. prepared porous nanostructured $Mn_2O_3$ electrodes by Mn-BTC-MOF calcination. A specific capacitance of 250 F $g^{-1}$ at a current density of 0.2 A $g^{-1}$ was obtained in a three-electrode system.[42]

It is worth commenting that despite metal oxides produced from MOF calcination have presented high electrochemical performance, very often these oxides lack enough structural stability, due to the volume expansion suffered throughout the charge-discharge process. In these cases, the addition of a second component as a stabilizing agent has been proposed to maintain the stability of these materials. Hence, carbon-based materials have been often proposed as matrix stabilizers of metal oxides, since they can form efficient composites, increase electrical conductivity and possess a considerable surface area. Recent work on this subject has shown, for instance, that reduced graphene oxide (rGO)-$Co_3O_4$ nanocomposites exhibit a high electrode stability after multiple charge-discharge cycles. The synergic effect between the MOF-derived $Co_3O_4$ hexagons and r-GO sheets as carbon matrix was determinant not only for the high cycling stability demonstrated, but also for an improved efficiency (Figure 2). Thus, the rGO-$Co_3O_4$ electrode material retained 80.5% of its specific capacitance after 5000 cycles of charge-discharge. Moreover, the specific capacitance of this hybrid electrode material was of 1300 F $g^{-1}$ in 0.1 M KOH electrolyte and a current density of 4 A $g^{-1}$. This good performance correlates with the high surface area and appropriate pore volume in the composite material.[43]

Metal sulfides are also of great interest for energy storage, among other applications, due to their natural abundance and electrochemical performance. However, they have limited applications in SCs due to their low structural and chemical stability. MOF-derived metal sulfides have been reported as electrode materials to overcome this issue.

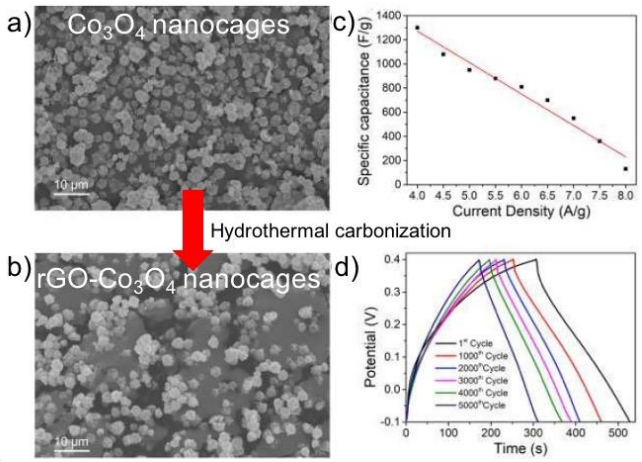


**Figure 2.** SEM images of the $Co_3O_4$ nanocages (a) and the (rGO)-$Co_3O_4$ nanocomposites (c). Specific capacitance plot with the current density of a (rGO)-$Co_3O_4$ electrode (b) and stability of overlaid GCDs of 1, 1000, 2000, 3000, 4000 and 5000 cycles at 4 A $g^{-1}$ in 0.1 M KOH. Reproduced with permission from Ref.[43] Copyright 2018, The Royal Society of Chemistry.

The porous nanostructures obtained through the MOF template synthesis can enhance the structural stability as well as the active sites density, improving the specific capacitance and cycle performance, simultaneously.[44] For instance, MOF-derived $Co_9S_8$ nanoparticles embedded in N, S-doped carbon were obtained from Co-MOF pyrolysis in the presence of thioacetamide, and tested as electrode material for SCs (Figure 3). The N, S-doped carbon wrapping the Co sulfide improved the electrode performance by enhancing the stability, while shortening the ion diffusion paths. The $Co_9S_8$/N,S-C material exhibited a high specific capacitance of 734 F $g^{-1}$ at a current density of 1 A $g^{-1}$ and a superior cycling stability. A capacitance retention of 99.8% after 140000 cycles at a current density of 10 A $g^{-1}$ was demonstrated, what is a remarkable achievement for metal sulfides.[45]

MOF conformal hydrolysis in which the original MOF morphology is retained has been recently reported as an exciting synthetic strategy to obtain porous metal hydroxides.

The metal hydroxides formed with this strategy have been used as electrode materials for SCs, and evaluated in large scale demonstrating to be cost-effective and highly efficient. In a recent example by Zhang et al., Ni-MOF-74 was utilized as precursor and hydrolyzed in the presence of KOH at various temperatures. The results indicated that temperature is a key parameter, Ni-MOF-74 being fully hydrolyzed to nickel hydroxide at an optimal temperature of 75 ºC (Figure 4).

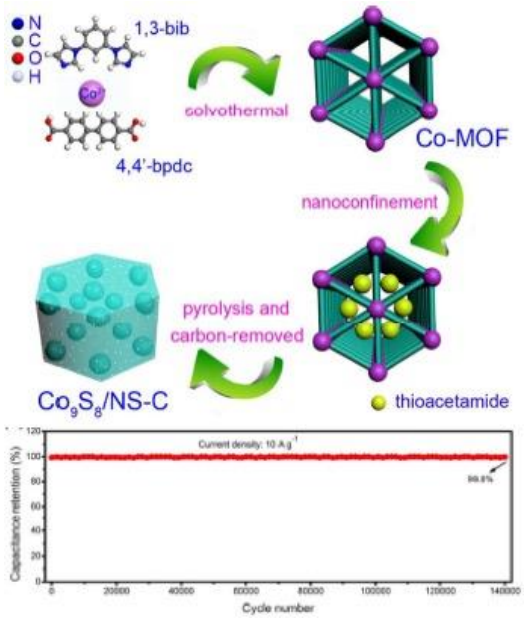


**Figure 3.** MOF templated synthesis of $Co_9S_8$/S,N-C and its cycling performance at 10 A $g^{-1}$ current density. Reproduced with permission Ref. [45] Copyright 2017, The Royal Society of Chemistry.

Incomplete hydrolysis occurring at other temperatures contributes to the formation of organic species, preventing the permeation of hydroxyl ions into the pores. Under optimal conditions, the resulting nickel hydroxide obtained with this interesting strategy showed the best electrode performance, exhibiting a specific capacitance equal to 713.2 C $g^{-1}$ at a current density of 1 A $g^{-1}$.[46]

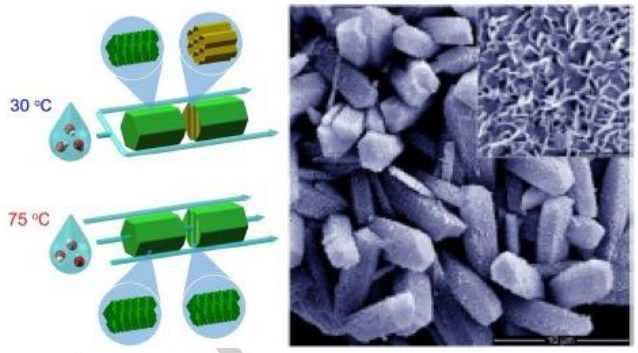


**Figure 4.** Scheme of Ni-MOF-74 hydrolysis to $Ni(OH)_2$ under optimal conditions (left) and SEM images of Ni-MOF-74 derived $Ni(OH)_2$ electrode material. Reproduced with permission from Ref.[46] Copyright 2017, American Chemical Society.

## 3. Properties of MOF derived bimetallic materials.

The rational design and synthesis of MOFs with tailored compositions and structures can serve as a toolbox to develop a wide array of MOF-derived structured functional materials. Specifically, bimetallic MOFs can be used to obtain novel electrodes for SCs that exhibit improved electrical energy storage performance.[34] The main challenges faced by monometallic MOF-derived electrodes for SCs are their poor rate capability and low stability.[47] The higher stability and performance reported for bimetal comprising MOFs compared with monometallic MOFs have been attributed to the unique "synergies" or "double function mechanism" between two different metal elements.[34] The rationale behind coupling two different metal cations derives from the expected increase in electrical conductivity and the possibility to carry out redox reactions between the metal centers allocated in the MOF structure. It is well-known that two metal centers in a given MOF can cause distinctive electrochemical behavior due to the different redox potentials and respective electronic configurations.

Thus, for instance, in those cases in which the main contribution to the activation energy of the rate determining step in a mechanism is electron transfer between the active site and the adsorbate, the presence of two metals may favor this electron transfer due to the better overlap of atomic orbitals and the modification of the electrochemical potential. Consequently, bimetallic MOFs derived materials offer more opportunities than monometallic electrodes in SCs.[48]

The main aim of the present review is to present the considerable information currently available on the superior performance of MOF-derived bimetallic nanostructures in the field of SCs. Table 1 summarizes the most relevant MOF-derived bimetallic electrode materials indicating the reported performance as SCs. The aim of this review is to attract further interest of the readers by showing the opportunities and challenges in this field.

**Table 1.** List of bimetallic MOF templates and their derived materials with a summary of the main capacitive data in SC application.

| MOF | Derived material | Specific capacitance ($Fg^{-1}$) | Energy density (Wh $Kg^{-1}$) | Power density (W $Kg^{-1}$) | Ref |
|---|---|---|---|---|---|
| **Ni/Co-MOF-74** | $Ni_xCo_{3-x}O_4$ | 797 | 27.7 | 5000 | [49] |
| **Ni/Zn-MOF** | NiO/ZnO | 435.1 | - | - | [50] |
| **Yolk-shell Ni/Zn-MOF** | NiO/ZnO hollow sphere | 497 | - | - | [51] |
| **Zn/Co-MOF** | Zn-Co-S/NF nanosheets | 2354.3 | 31.9 | 850 | [52] |
| **Zn/Co-ZIF** | Zn-Co-S | 1266 | - | - | [53] |
| **Ni/Co-MOF-5** | Ni/Co-S NPs | 1377.5 | 36.9 | 1066.4 | [54] |

| | | | | | |
|---|---|---|---|---|---|
| **Ni/Co-ZIF-67** | $Ni_{3x}Co_{3-3x}S_4$ | 696 | 7 | 100.4 | [55] |
| **Ni/Zn-BDC MOF** | $NiS_2$/ZnS | 1198 | 28 | 748.9 | [56] |
| **Mn/Mo-MOF** | MnS/$MoS_2$/ C hybrid | 1162 | 31 | 388.3 | [57] |
| **Co/Mn-MOF-74** | Co/$MnO_x$@ C | 800 | - | - | [58] |
| **NiCo-MOF-74** | NiCo-hydroxides | 875.3 C $g^{-1}$ | 81 | 1.9 | [59] |
| **NiCo-MOF** | $NiCo_2O_4$/β-$Ni_xCo_{1-x}(OH)_2$/α-$Ni_xCo_{1-x}(OH)_2$ | 1315 | 36.98 | 801.5 | [60] |
| **Co/Zn-ZIF** | Nanoporous carbon | 10.5 | - | - | [61] |
| **Zn/Zr-MOF** | HP-Uio-66 | 849 | 32 | 240 | [62] |
| **$NiCo_2O_4$ + ZIF8** | $NiCo_2O_4$@NCP | 310 | 28 | 850 | [63] |
| **Ni and Co MOF + rGO** | Ni/Co/rGO | 860 | 72.8 | 850 | [64] |
| **CoNi-MOF** | $Ni_xCo_{1-x}(OH)_2$ | 1235.9 | 21.9 | 348.9 | [65] |
| **ZIF-67** | $CoNi_2S_4$ | 1890 | 35 | 640 | [66] |
| **Ni/Co-ZIF-67** | $NiCoSe_2$ | 300.2 | - | - | [67] |
| **Co/Ni-MOF-74** | $NiCo_2O_4$ | 732 C $g^{-1}$ | 46.9 | 425.3 | [68] |
| **CuFeBTC** | CuFeBTC/S-GNS | 1164.3 | 96.57 | 1545.12 | [69] |
| **NiCo-MOF** | **NiCoP/C** | **775.7** | **47.6** | **798.9** | [70] |

## 4. MOF derived bimetallic electrode materials

Nanostructured materials for electrical energy storage in SCs must exhibit different properties in terms of electrical conductivity, significant surface area and controlled pore size, among others.[48] In this regard, in spite of the large specific surface area, the usually very poor electric conductivity of MOFs result in low electrochemical efficiency and low specific current. It is the hope in the area that electrically conductive MOFs could be prepared in the future.

Meanwhile, alternatively, MOFs can be used as templates to obtain controlled nanostructured electrodes that have shown superior capacitative data in electrical energy storage compared to other materials.[35b, 35d, 35e, 71]

In this context, recent progress in the preparation of bimetallic MOFs has allowed to obtain the corresponding bimetallic materials exhibiting high crystallinity and porosity.[72] Moreover, starting from the bimetallic MOF, most of these methods require a single-step easy procedures and can be up scaled in a reliable way to the pilot and industrial scale .[73] Accordingly, many different nanostructures have been obtained from bimetallic MOFs as templates.[74] This section presents the different types of nanostructured materials obtained from bimetallic MOFs directly submitted to different synthetic protocols or as components in nanocomposites. Their performance as electrode materials in SCs is also summarized.

### 4.1. MOF derived bimetallic mixed metal oxides.

Hybrid metal oxides of general formula $AB_2O_4$ have received increasing interest in recent years, because their chemical composition allows large flexibility to improve the new electrical, chemical and magnetic properties, as compared to monometallic oxides.[75] The origin of performance improvement is the existence of two different metallic species with multiple valences and the synergism arising from them. However, controlled production of the mentioned materials by other procedures different from MOF transformation is still a serious problem.[76]

Hybrid metal oxides have also shown superior characteristics (i.e. potential window, conductivity, active sites, stability) in electrical energy storage than the individual components separately, attributed to a synergistic effect of bimetallic redox species.[77] These redox species play a central role improving the electrochemical efficiency of SCs.

One of the main issues to be addressed in the use of metal oxides as electrodes in SCs is the poor electrolyte diffusion length within the metal oxides pores. It has been demonstrated that diffusion of electrolyte species within the pores of highly crystalline metal oxides is restricted to 20 nm, approximately. However, similar electrolyte compositions were able to diffuse larger distances in amorphous oxide materials (approximately 50 nm).[78]

Since the observed crystallinity of MOFs-derived metal oxides is significant, the diffusion restrictions of electrolyte within their pores is expected to be high too. Decreasing the crystallinity of MOF-derived metal oxides should lead to electrolyte mean diffusion distance enhancement.[79] Besides crystallinity, pore dimension is also a crucial parameter controlling electrolyte diffusion. Tuning the pore dimension of the materials to the electrolyte ion size via MOFs architecture engineering and/or post-synthetic treatment is also important to facilitate ion diffusion.

Recently, MOF-derived bimetallic metal oxides with two different metals in the same framework have been extensively studied because of their considerable surface area, allowing a high interfacial electrode/electrolyte contact, and flexibility in the precise control of the composition. Furthermore, MOF-derived bimetallic metal oxides have demonstrated improved electric conductivity than the individual metal oxides.[80] Since bimetallic MOFs have very adjustable metal ions and organic ligands, as well as extremely adaptable porosity and surface area, they are very convenient templates for constructing nanoporous hybrid metal oxides with extremely tailorable compositions, structures, and features to satisfy industrial demands.

So far, the number of bimetallic metal oxide nanostructures that have been expertly produced from bimetallic MOFs and investigated in detail is not large in comparison with MOF-derived carbons. However, available data have revealed very promising performance for electrical energy storage. In this

regard, $Ni_xCo_{3-x}O_4$ NPs have been synthesized from bimetallic Ni/Co MOF-74 by calcination in air at 400 ºC, investigating the electrochemical characteristics of $Ni_xCo_{3-x}O_4$-based electrodes as function of Ni/Co.[49] In this study, five single-phase isostructural MOF-74 samples of Ni/Co atomic ratios from infinite to zero were synthesized (Figure 5 a), resulting in $Co_3O_4$, NiO, and three mixed metal oxides with different Ni/Co ratio ($Ni_xCo_{3-x}O_4$).[49]

The measured areas from the CV plots for the mixed metal oxides ($Ni_xCo_{3-x}O_4$) were higher than that of NiO and $Co_3O_4$, indicating that the $Ni_xCo_{3-x}O_4$ materials presented enhanced capacitance than single metal oxides. The sample with the highest capacitance value (797 F $g^{-1}$) corresponded to a Ni/Co ratio of 1, while oxides with Ni/Co ratios of 3 and 5 exhibited 493 and 332 F $g^{-1}$, respectively (Figure 5 a).[49] This trend was explained as derived from the decrease in conductivity as the Ni content increases due to the variation in the electron transfer activation energy between cations, as reported elsewhere.[81]

In a similar approach, Yu *et* al. reported the rational design and solvent-free synthesis of Co/Ni-MOF-74 and subsequent calcination, obtaining hybrid metal oxides as nanowires. The authors reported different phases depending on the Ni/Co ratio. Electrochemical measurements indicated that the hybrid metal oxide $NiCo_2O_4$ exhibited superior specific capacity (732 C $g^{-1}$ at a current density of 1 A $g^{-1}$) than the $Co_3O_4$ and NiO monometallic oxides. ASD were built using the Co/Ni-MOF-74 derived as electrode material, achieving a specific energy density of 46.9 W h $Kg^{-1}$ at a specific power density of 425.3 W $Kg^{-1}$ with remarkable cycling performance. [68]

In different approach, Yang *et al*. used a bimetallic Zn/Ni MOF as the precursor of hierarchical ZnO/NiO microstructures.[50] It was observed, that the seaweed-like morphology of the Ni/Zn-MOF precursor completely changed after calcination forming ZnO/NiO nanosheets (Figure 5 b). According to the authors, this particular morphology presents an improved ionic and electronic conductivity. Therefore, the faster ion diffusion and electron transfer at the working electrode reduced the charge-transfer resistance within the nanosheets (Figure 5 b).[50] As consequence, a specific capacitance of 435.1 F $g^{-1}$ when the current density is equal to 1 A $g^{-1}$ was obtained for ZnO/NiO composites.

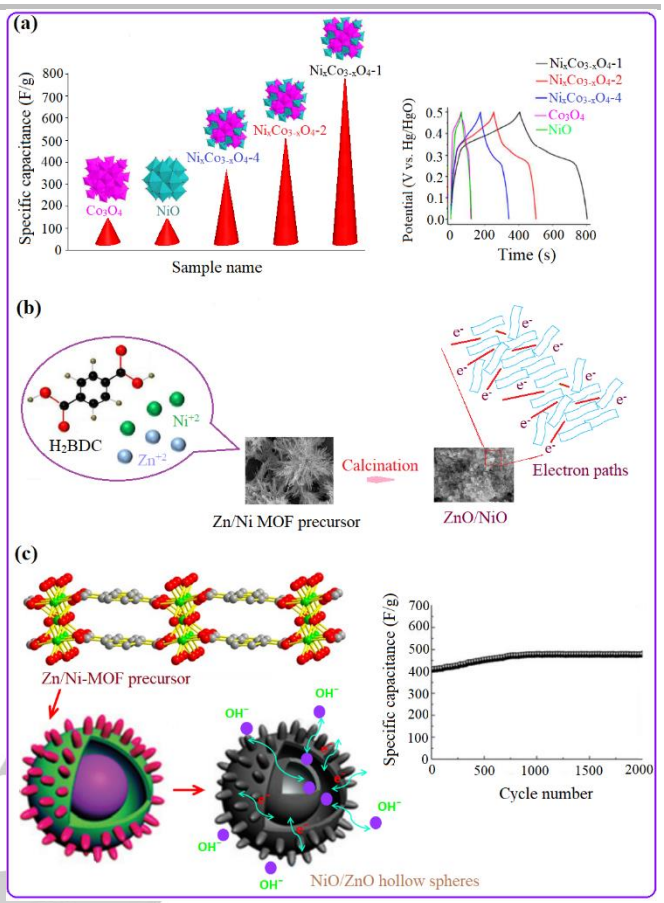


**Figure 5.** (a) Various metal oxide materials derived from bimetallic MOF-74 crystals and GCD curves at a current density of 1 $Ag^{-1}$ for NiO, $Co_3O_4$, $Ni_xCo_{3-x}O_4$-1, $Ni_xCo_{3-x}O_4$-2 and $Ni_xCo_{3-x}O_4$-4. (b) schematic illustration of ZnO/NiO derived from MOF-74 as an electrode material in SCs. (c) double-shelled NiO/ZnO hollow spheres and its cyclic performance at the current density of 5.2 A $g^{-1}$ for 2000 cycles. (a) Reproduced with permission from Ref.[49] Copyright 2015, the Royal Society of Chemistry. (b) Reproduced with permission from Ref.[50] Copyright 2018, Elsevier Inc, (c) Reproduced with permission from Ref.[51] Copyright 2016, the Royal Society of Chemistry.

Besides easy reliable control on the atomic ratio, MOFs as templates can also serve to obtain double metal oxide particles with defined specific morphology, particularly suited to build high performing SCs. As an example, Li *et al*. used a Ni/Zn-MOF as a precursor to synthesize a novel kind of hierarchical double-shelled NiO/ZnO hollow sphere (Figure 5 c).[51] The main advantages of the double-shell NiO/ZnO hollow sphere morphology are that the ions and electrons can be easily transferred at the interface of electrode/electrolyte and that the volume changes occurring during the charge-discharge processes can be easily managed with the hollow spherical morphology. It was proposed that the unique double-shelled NiO/ZnO hollow structures allowed free space for accommodating the volume modification over the insertion and desertion ion. Therefore, efficient SC devices based on this double-shelled spheres can be anticipated.[82]

Indeed, these hollow spheres were applied as electrodes in SCs exhibiting a remarkable capacitance of 497 F $g^{-1}$ when the current density was equal to 1.3 A $g^{-1}$.[51] The capacitance of the NiO/ZnO electrodes raised progressively from 408 to 478 F $g^{-1}$ over the first 800 cycles. Similar improvement during the initial cycling has been previously observed and attributed to the activation of some additional sites on the material surface.[83] It is

also worth commenting that almost no degradation in the subsequent 1200 charge-discharge cycles was observed, indicating a good cycling stability. Furthermore, accessibility of electrolyte ions through the paths together with activation of surface sites were identified as the most important factors responsible for the electrochemical behavior of this SC electrode.[51]

#### 4.2. MOF derived bimetallic mixed metal chalcogenides

Transition metal sulfides, including $FeS_2$, $MoS_2$, NiS, and CoS, among others, have attracted considerable attention as promising materials in different fields such as solar and fuel cells, optoelectronic, thermoelectric, memory and energy storage devices.[84] Transition metal sulfides are also considered as very promising electrodes in SCs, due to their predicted energy storage capacity as well as their enhanced electrical conductivity.[85] However, transition metal sulfides have typically shown as main drawbacks in SCs slow charging/discharging rates and low cycling stability.

Compared to monometallic sulfides, binary metal sulfides such as $FeCo_2S_4$, $MnCo_2S_4$, and $NiCo_2S_4$, have demonstrated improved electrochemical response and capacitance than monometallic sulfides[86] as consequence of a more favorable orbital overlap and adequate charge relocation between diverse ions, both factors decreasing the kinetic energy barriers.[87]

Conversion of bimetallic MOFs, with different metal centers homogeneously distributed, appears as an appealing procedure to obtain transition metal sulfides with controlled composition and particle morphology. For instance, amorphous $CoNi_2S_4$ nanocages were synthesized from ZIF-67 by Wang *et al*.[66] Their study revealed that the $CoNi_2S_4$ nanocages have significantly better electrochemical response as electrode than CoS, and the improved performance was attributed to the $CoNi_2S_4$ unique structure. The $CoNi_2S_4$ morphology presents a high specific surface area which increases with the nanosheet size on the $CoNi_2S_4$ nanocage shell, increasing the electrode-electrolyte interfacial area. This unique structure favored $OH^-$ ions movement from the electrolyte solution to the electrode surface, accelerating Faradaic reactions and enhancing the capacitance (Figure 6 a). $CoNi_2S_2$ nanocages and yolk-shell (YS) carbon were used as cathode and anode materials, respectively, in a $CoNi_2S_2$/YS-CS ASC, demonstrating a good energy of 35 W h $kg^{-1}$ at a power density of 640 W $kg^{-1}$.[66]

In a different example, Tao *et al*. prepared 2D bimetallic zinc-cobalt MOFs (Zn/Co-MOF) nanosheets with leaf-like morphology supported on a Ni foam and, after sulfurization, porous zinc cobalt sulfide nanosheets array on Ni foam (Zn-Co-S/NF) were obtained.[52] For comparison purposes, a zinc cobalt sulfide powder (Zn-Co-S-P) was also prepared as reference electrode for SC. The electrochemical characteristics of Zn-Co-S-P and Zn-Co-S/NF were examined using CV and GCD curves in a three-electrode cell with 1 M KOH electrolyte. Figure 6 c presents the characteristic CV curves corresponding to Zn-Co-S-P and Zn-Co-S/NF at a scan rate of 10 mV $s^{-1}$ in the voltage window from to -0.1-0.6 volts (versus SCE). Two redox peaks were recorded in the CV curves in both Zn-Co-S-P and Zn-Co-S/NF, corresponding to reversible Faradaic redox reactions correlated with MS/M-S-OH, where M is zinc or cobalt. As presented in Figure 6 d, the as-prepared Zn-Co-S/NF nanosheets array displayed much better capacitance value and stability than the Zn-Co-S-P, obtaining 2354.3 F $g^{-1}$ and 88.6 % capacitance retention after $10^3$ cycles, while 355.3 F $g^{-1}$ and 75.8 % retention were measured for Zn-Co-S-P. The improved capacitance and stability were attributed to the better electric conductivity, mechanical stability, larger density of electroactive sites, and ease transference of electrolyte ions and electrons for Zn-Co-S/NF endowed by the arrangement of the nanosheets array (Figure 6 b). Furthermore, a high energy density of 31.9 W h $kg^{-1}$ at a power density of 850.0 W $kg^{-1}$ was measured from an all-solid-state, Zn-Co-S/NF//AC/NF ASC, using AC/NF as anode and Zn-Co-S/NF as cathode.[52]

The rational design of proper nanostructures for electrode materials can significantly increase their electrochemical performance. For instance, it has been demonstrated that hollow structures can be very convenient regarding electrode performance, since they present remarkable surface area, shortened diffusion pathway, reduced subunit aggregation and high density of active sites for charge transfer.[14b] In this regard, zinc-cobalt sulfide rhombic dodecahedral cages (Zn-Co-S RDCs) were synthesized with well-defined single or double-shelled hollow structures through a continuous MOF chemical etching and sulfurization method by Zhang *et al*.[53] TEM images of these materials are presented in Figure 7 a, illustrating the remarkable morphology and structuring that can be achieved by transformation of MOFs. It seems that double-shelled hollow structure impedes material aggregation, maximizing the specific surface area. On the other hand, the high surface area in the double-shelled hollow structures exposes a larger number of electroactive sites enhancing the charge transfer rate and, in overall, improving its electrochemical performance. It is worth commenting the robustness of this structure as consequence of the interconnection of adjacent shells conferring high cyclic stability (Figure 7 b). Derived from nanostructuring and composition, Zn-Co-S RDCs exhibited a specific capacitance of 1266 F $g^{-1}$ at 1 A $g^{-1}$ current density in a battery-like electrode setup.[53]

It is well-known that there is a correlation between material porosity and their electrochemical efficiency. This is due to the electron and ion easy relocation at the electrode/electrolyte interface, as well as a flexible accommodation of the volume modification occurring in the charge-discharge processes.[84] Bimetallic MOFs (Ni/Co-MOF-5) with nanosheet-assembled, flower-like structure via etching nickel-MOF microspheres in a CoNi solution were synthesized by Chen *et* .al (Figure 8 a).[54] Subsequent Ni/Co-MOF-5 sulfurization renders Ni/Co-S NPs that were employed as electrodes for SCs.

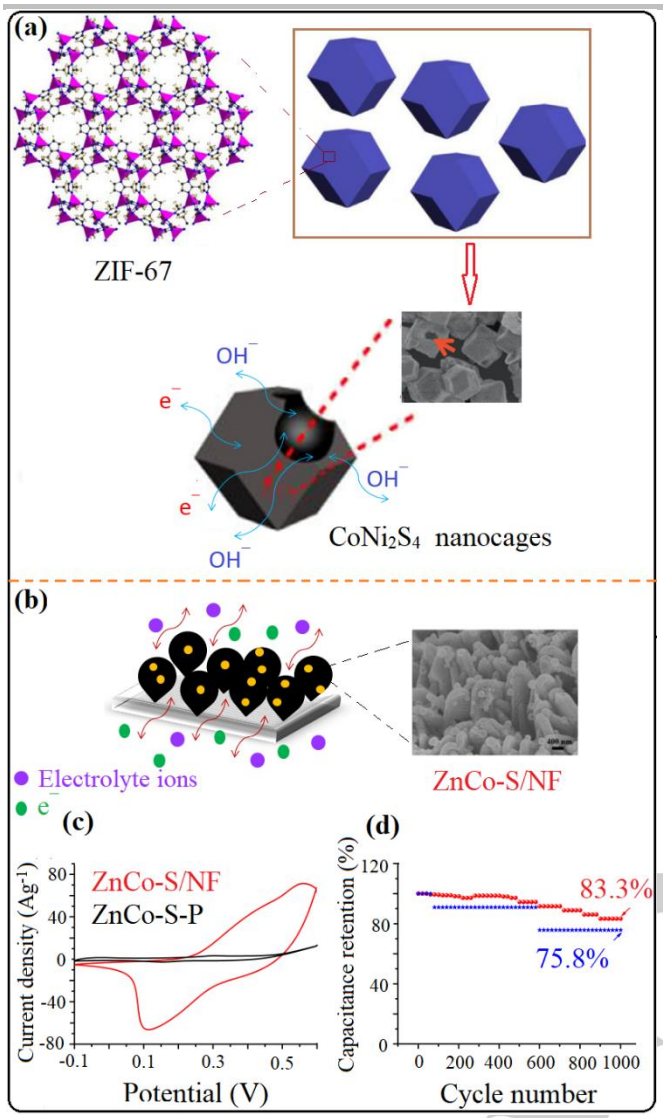


**Figure 6.** (a) The electrochemical performance of $CoNi_2S_4$ nanocages derived from ZIF-67, (b) SEM image of ZnCo-S/NF (NF: nickel foam) electrode material and its electrochemical performance, (c) CV curves corresponding to Zn-Co-S-P (P: powder) and Zn-Co-S/NF at a 10 $mVs^{-1}$ scan rate in a three electrode cell, and (d) The cyclic behavior of Zn-Co-S-P and Zn-Co-S/NF for 1000 cycles. (a) Reproduced with permission from Ref.[66] Copyright 2017, Elsevier Inc, (b-d) Reproduced with permission from Ref.[52] Copyright 2018, John Wiley & Sons, Inc.

The Ni/Co-S electrodes demonstrated a high capacity (1377.5 F $g^{-1}$ at a current density of 1 $Ag^{-1}$) in spite of its low BET surface area (19.5 $m^2g^{-1}$). Moreover, 93.7 % of its initial specific capacitance was maintained after 3000 cycles (Figure 8 b). Further evaluation of the practical applications of Ni/Co-S material for SCs was carried out with a Ni/Co-S//AC ASD. Ni/Co-S//AC ASD exhibited an energy density of 36.9 W h $kg^{-1}$ at a power density of 1066.42 W $kg^{-1}$.[54]

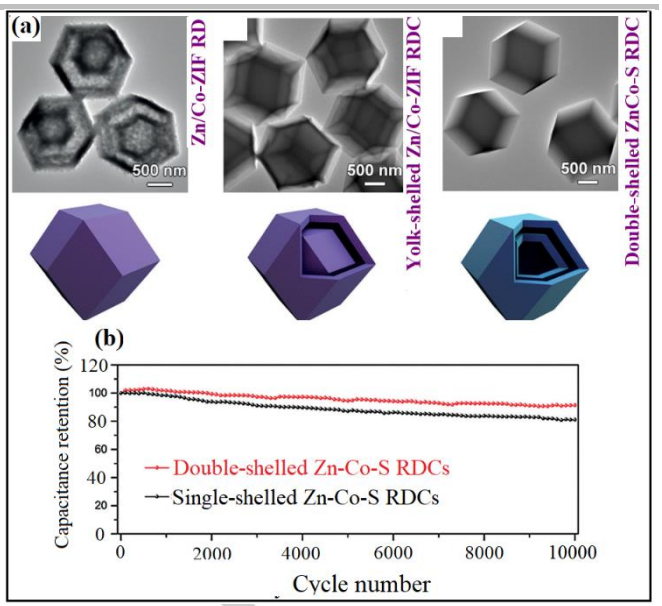


**Figure 7.** (a) TEM images of ZnCo-ZIF RD, yolk-shelled Zn/Co-ZIF RDC and double shelled ZnCo-S RDC materials, and (b) Cyclic stability of single shelled ZnCo-S RDC and double shelled ZnCo-S RDC electrode materials for 10000 cycles. Reproduced with permission from Ref.[53] Copyright 2017, John Wiley & Sons, Inc.

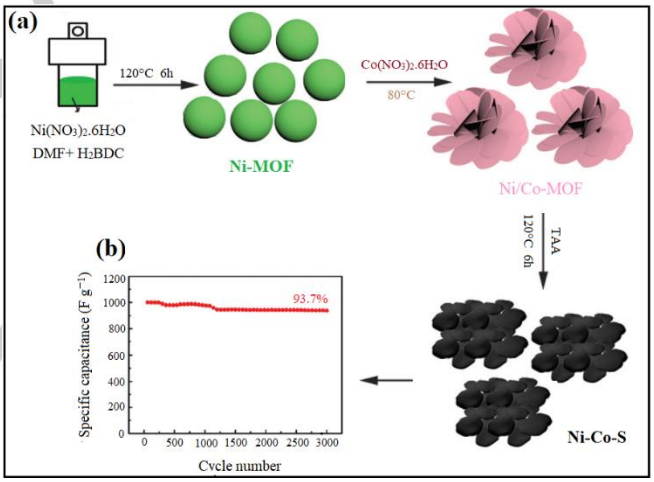


**Figure 8.** (a) Synthesis process of NiCo-S from NiCo-MOF (TAA: thioacetamide), and (b) Cyclic stability of NiCo-S for 3000 cycles. Reproduced with permission from Ref.[54] Copyright 2018, the Royal Society of Chemistry..

Synergistic effects between two or more materials in an electrode is an additional strategy to further enhancing energy storage efficiency. In this regard, Li *et* al. reported Ni/Zn-BDC (BDC:1,4-benzenedicarboxylate) MOF synthesis and subsequent sulfurization obtaining $NiS_2$/ZnS hollow nanospheres and their application as electrode material for high-performance SC (Figure 9).[56]

The well-defined voltage plateaus in the GCD plots revealed battery-like features. The excellent symmetry of all the GCD curves showed remarkable electrochemical capacitance values and superior reversible redox processes at the electrode interphase. The specific capacitance for this electrode was equal to 1198 F $g^{-1}$ at a current density of 1 A $g^{-1}$, and this specific capacitance decreased only to 87 % from the initial one after 1000 cycles. The improved stability was attributed to the slight

peeling-off of the active materials in the electrode. The as-synthesized electrodes were included in ASD, displaying high energy density and power density values (28.0 W $kg^{-1}$ and 748.9 W h $kg^{-1}$, respectively) (Figure 9 c and 9 d).[56]

The exceptional electrochemical efficiency achieved with the $NiS_2$/ZnS hollow nanospheres was attributed to different reasons. On one hand, the easy electron/ion relocation as well as the measured capacitance value must be attributed the synergism between $NiS_2$ and ZnS. On the other hand, ions/electrons are able to access the inner sphere void space, and consequently, their diffusion length to the electrode is shortened by the mesoporous hollow structure, resulting in an enhanced efficiency.[56]

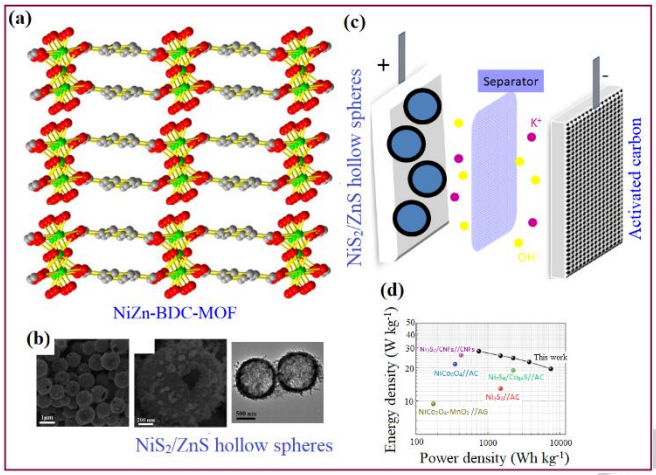


**Figure 9.** (a) Structure of NiZn-BDC-MOF, (b) SEM and TEM image of $NiS_2$/ZnS hollow spheres, (c) schematic illustration of the $NiS_2$/ZnS hollow spheres //AC ASD, and (d) Ragon plot of $NiS_2$/ZnS hollow spheres //AC ASD**.** Reproduced with permission from Ref.[56] Copyright 2016, the Royal Society of Chemistry..

In the previous paragraphs it has been shown that transition metal oxides and sulfides exhibit high capacitance and energy density values, making these materials suitable for energy storage application. Selenium, sharing the same group as oxygen and sulfur in the Periodic Table, is expected to provide a similar chemical behavior. However, due to the lower Se electronegativity, it can be anticipated that selenides will be able to promote faster electron transfer reactions than oxides and sulfides. An improved electrochemical response of selenides could also be envisioned considering their higher electron conductivity, defined redox response, and larger cycling stability of these chalcogenides. Furthermore, analogously to the case of oxides and sulfides, it is also expected that bimetallic selenides should also exhibit better electrochemical performance than monometallic selenides due to the synergism arising from the presence of two metal centers. Therefore, bimetallic MOFs derivatives can also be good candidates as templates of bimetallic selenides.

Accordingly, Ni/Co-ZIF-67 has been recently reported as a precursor for the synthesis of $NiCoSe_2$.[67] This material possesses polyhedral structure and presents a large specific area. Electrochemical characterization showed that this material possess a specific capacitance of 300.2 F $g^{-1}$, at a current density of 1 $Ag^{-1}$. Moreover, the Ni/Co-ZIF-67-derived material showed an outstanding stability, and a remarkably 100 % of the $NiCoSe_2$ electrode capacitance was maintained after 2000 cycles.[67]

### 4.3. MOF derived bimetallic double hydroxides

Similarly to the corresponding oxides, transition metal hydroxides have also been considered as promising electrode materials for SCs due to their huge theoretical capacitance values in the range of 3500−4600 F $g^{-1}$.[59, 89] A powerful approach to increase even further the electrochemical efficiency of metal hydroxides is introducing additional metal ions (such as $Al^{3+}$, $Co^{2+}$, $Mo^{2+}$, and $Mn^{2+}$) to obtain multimetallic hydroxides. Different studies have confirmed that introduction in a monometallic hydroxide an additional metal generates structural defects that result in an increase in the conductivity and the rate of redox reactions, with an overall improvement of the electrochemical response.[90]

In one of these few studies, $Ni_xCo_{1-x}(OH)_2$ microspheres of uniform dimensions were prepared by He *et al.* in alkali solution using a bimetallic CoNi-MOF as both self-sacrificing template and precursor.[65] The CoNi-MOF conversion procedure promoted microsphere porosity, increasing the pore volume and BET surface area. Thus, the $Ni_xCo_{1x}(OH)_2$ microspheres exhibit a large buffer space able to accommodate volume expansion occurring in the charging/discharging cycles as well as provide preferential pathways for electrons and ions to reach electrode/electrolyte interphase, both features contributing positively to increase the electrochemical efficiency and stability.

CV measurements with monometallic MOFs-derived $Co(OH)_2$ and $Ni(OH)_2$ were carried out for the sake of comparison. The appearance of two and one couple of redox peaks was attributed to the reversible redox reactions of $Co(OH)_2$ and $Ni(OH)_2$, respectively.[90a] A down-shift to negative values was observed in the MOF-derived $Ni_xCo_{1-x}(OH)_2$ oxidation and reduction potentials in comparison with the MOF derived $Ni(OH)_2$, leading to propose an easier charging process in double $Ni_xCo_{1-x}(OH)_2$ hydroxide electrodes respect to the monometallic $Ni(OH)_2$. The redox potential down-shift was attributed to the appearance of a synergistic effect between the different metal centers and from the higher electrical conductivity of the double hydroxide. The measured specific capacitance of $Ni_xCo_{1-x}(OH)_2$ composite was of 1235.9 F $g^{-1}$ at 0.5 A $g^{-1}$.[65]

In a different approach, Qu *et al.* synthetized different of highly porous MOF-derived double hydroxides submitting to a facile alkaline treatment procedure a series of CoNi MOF-74 with different Co/Ni ratios as precursors.[59] High porosity and large surface area were measured in these double hydroxides. Additionally, they presented enhanced electrochemical efficiency attributed to their hierarchical porous structure and the presence of interlayer functional groups. SEM images of the synthetized Ni/Co double hydroxide (Ni/Co-MDH) presented spear-like morphology (Figure 10 a). According to the authors, this morphology facilitates the electron transfer and electrolyte ion migration in redox reactions. ASD with a Ni/Co-MDH//N-C configuration were tested, measuring a remarkable cyclic stability and Coulombic efficiency as can be observed in Figure 10 b.[59]

It is fair to note that although several binary hydroxides display better electrochemical efficiency than analogous monometallic materials,[91] there are cases in which bimetallic hydroxides have shown lower conductivity and smaller cycling efficiency than their individual metal hydroxides.[92] To overcome these issues found in those bimetallic hydroxides, attempts have

been made to design heterojunctions by mixing hydroxides with other materials, such as metal oxides or different metal hydroxides, with high structural stability and electrical conductivity.[93]

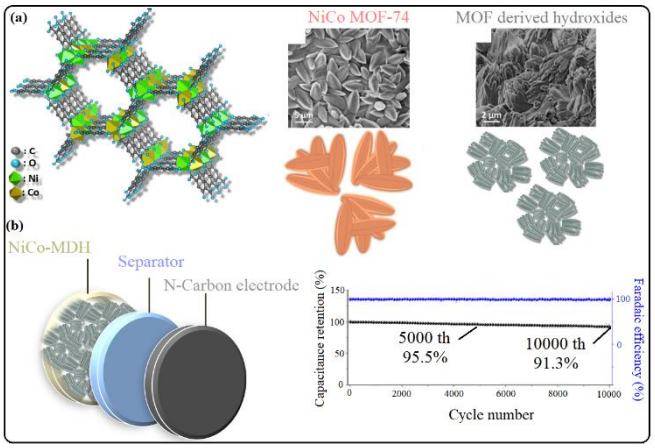


**Figure 10.** (a) Structure of Ni/Co-MOF-74 and SEM images of Ni/Co-MOF-74 and MOF derived hydroxides and (b) schematically illustration of asymmetric device and cyclic stability at 13.5 A $g^{-1}$ for 10000 cycles. Reproduced with permission from Ref.[59] Copyright 2017, American Chemical Society.

In this context, an accordion-like ternary $NiCo_2O_4$/β-$Ni_xCo_{1-x}(OH)_2$/α-$Ni_xCo_{1-x}(OH)_2$ material was synthetized from a bimetallic Co/Ni MOF as a sacrificial template through a sequential alkaline hydrolysis and oxidation reaction (Figure 11 a).[60] Upon MOF soaking in alkaline solution the diffraction peaks characteristic to the parent MOF vanished, while those corresponding to Co/Ni hydroxides appeared. A selective oxidation with $H_2O_2$ was subsequently carried out. This treatment leads to the appearance of the distinctive peaks of the (440), (400), (311) and (200) planes of $NiCo_2O_4$ at 64.98°, 44.62°, 36.69° and 31.15° together with the specific diffraction peaks related to α- and β-$Ni_xCo_{1-x}(OH)_2$, as presented in Figure 11 a.[60]

The electrochemical responses of the MOF-derived bimetallic hydroxide $Co_x/Ni_{1-x}(OH)_2$ and the ternary $NiCo_2O_4$/β-$Ni_xCo_{1-x}(OH)_2$/α-$Ni_xCo_{1-x}(OH)_2$ material were evaluated. The CV curves for the MOF-derived bimetallic hydroxide $Co_x/Ni_{1-x}(OH)_2$ showed a lower oxidation potential than those of the corresponding monometallic hydroxides. This shift was taken as an indication of the interaction between $Ni^{2+}$ and $Co^{2+}$ ions.[91b] Capacitance measurements indicate that the optimal Co/Ni ratio is 3:1. However examination of the $Ni_xCo_{1-x}(OH)_2$ (x = 0.25) cycling efficiency at 5 A $g^{-1}$ showed a 52% reduction of its specific capacitance after 2000 cycles, restraining its applicability considerably.[60]

In sharp contrast, the ternary $NiCo_2O_4$/β-$Ni_xCo_{1-x}(OH)_2$/α-$Ni_xCo_{1-x}(OH)_2$ material retained 90.7% of its specific capacitance after $10^4$ charge−discharge cycles at a current density of 5 A $g^{-1}$ (Figure 11 b), which is considerably more satisfactory than the stability of $Ni_{0.25}Co_{0.75}(OH)_2$. The increase in the diffusion pathway and the electrolyte migration rate observed in the fast charge/discharge cycles was attributed to the well-designed accordion-like structure of the $Ni_xCo_{1-x}(OH)_2$ nanosheets.[60] The morphology of the hierarchical structure was apparently protected during the charge/discharge cycling assessment by the volume provided by the voids and channels between nearby nanosheets. Additionally, the $NiCo_2O_4$ component played two significant roles. It served as scaffold supporting the accordion-like structure, but also contributed to facilitate electron migration.[60]

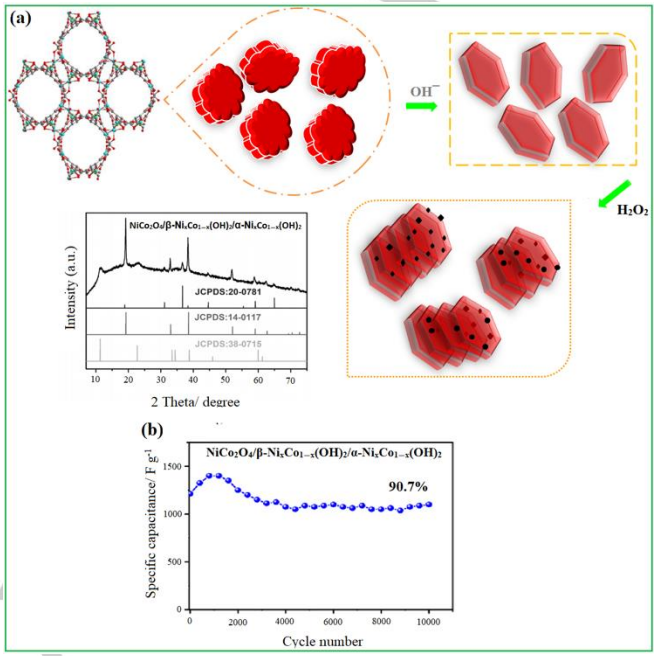


**Figure 11.** (a) Synthesis of accordion-like ternary $NiCo_2O_4$/β-$Ni_xCo_{1-x}(OH)_2$/α-$Ni_xCo_{1-x}(OH)_2$ and the corresponding XRD patterns, and (b) cycling stability of the $NiCo_2O_4$/β-$Ni_xCo_{1-x}(OH)_2$/α-$Ni_xCo_{1-x}(OH)_2$ electrode material. Reproduced with permission from Ref.[60] Copyright 2018, American Chemical Society.

### 4.4. Carbon materials derived from bimetallic MOFs

Carbon-based materials, frequently containing embedded metal nanoparticles, have been the most widely studied electrode materials in SCs, since they exhibit controllable morphology, tunable pore size, and adequate surface properties. Remarkable capacitance efficiency values have been achieved by controlling carbon porosity, particularly in EDLCs.[94]

MOFs are well-known to comprise both metal ions and organic linkers, which produce adaptable cavities with no need for templates. MOFs submitted to carbonization can induce directly porosity in the resulting carbon structure that incorporates metal nanoparticles in intimate contact with the carbon residue.

In one of the examples reported in the literature, mesoporous structures with considerable degree of carbon graphitization have been obtained from Co-ZIF-67 MOF.[95] However, this material has shown very low specific surface area and small nitrogen content. In contrast to these results with Co ZIF, the carbon residue obtained from analogous Zn-ZIF-8 exhibits a microporous structure, large specific surface area, and high degree of nitrogen doping,[96] although the degree of carbon graphitization was low. Continuing with the line of the review and as commented in the previous sections, materials derived from bimetallic MOFs overcome the performance of related monometallic analogues, derived from the synergy arising from the combination of two ions in one single material. Available literature data shows that the same rule is valid also for carbonaceous residues derived from MOFs.[97]

Thus, similarly to the previously commented case of Co and Zn ZIFs, nanoporous carbon residues have also been obtained from a bimetallic ($Zn^{2+}$ and $Co^{2+}$) ZIF as a precursor (Figure 12 a).[61] No presence of redox peaks in the CV curves was detected, hence, it was concluded that remaining Co and Zn do not contribute to the capacitive behavior. The GCD curves (Figure 12 b) of an asymmetric two-electrode cell were also measured, observing an asymmetric triangular shape what demonstrate the absence of an internal resistance drop. It was proposed that the main reason for this remarkable behavior was the evolution of carbon nanotubes (CNT) during the carbonization process, which increases electric conductivity and favors quick ion diffusion.[61]

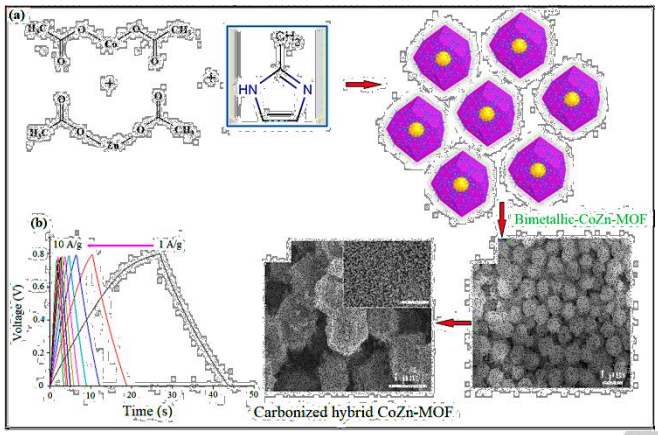


**Figure 12.** (a) Synthesis process and SEM images of CoZn-MOF and carbonized hybrid CoZn-MOF, (b) GCD curves of CoZn-MOF derived nanoporous carbon at various current densities. Reproduced with permission from Ref.[61] Copyright 2017, Elsevier Inc.

### 4.5. MOF derived bimetallic composites

Despite the efficiency improvement for energy storage in SCs demonstrated so far by materials derived from bimetallic MOFs as described in the previous sections, the short period of time elapsed since the initial reports clearly indicates that the research field on multimetallic materials derived from MOFs is still in its infancy, and many more findings are still to be expected. One research direction that will grow in the near future is the exploitation of the synergistic effects and unique features that can possible occur in composite materials. As one example, carbon matrices as supports of metal oxides have been found to efficiently decrease the mechanical stress typically occurring in metal oxides as well as to confer pseudocapacitive and EDLC properties in electrodes. Hence, carbon-supported metal oxides can attain superior stability in SC electrodes than pure metal oxides. Additionally, hybridizing metal oxides with carbon-based materials improves their energy density for ASD by expanding the potential window range.[98]

In recent years, bimetallic MOFs have demonstrated to be appropriate templates to obtain porous carbon−mixed metal oxide composites. In this transformation metal nodes become oxidized to mixed metal oxides and the organic linkers are converted into porous carbons. The most commonly reported MOF-derived bicomponent composites are bimetallic MOF-derived carbon-based composites, including bimetallic NP combinations, metal carbides, metal hydroxides or metal oxide NPs and carbonaceous materials.

For instance, the synthesis of Co and $MnO_x$ supported in nanoporous carbon matrix via Co/Mn-MOF-74 carbonization has been reported.[58] In this example, the synthesis of a new binary metal Co/Mn-MOF-74 sample was conducted by solvothermal synthesis under mild conditions. Depending on the carbonization temperature, in the range of 600-800 ℃, different porous metal/metal oxide@carbon (Co/MnO@C) samples were obtained, examining their performance as electrodes in SCs.[58] SEM images and elemental analysis mapping of these materials are shown in Figure 13 a.

The highest specific capacitance was achieved for porous Co/MnO@C-700 electrodes measuring a value of 800 F $g^{-1}$ at 1 A $g^{-1}$ current density. However, discharge at higher current density led to lower specific capacitance values, derived presumably from the increase of Co/MnO@C-700 internal resistance at large current densities and the involvement of spurious centers in the redox reactions, as it can be deduced from Figure 13 b.[58] Two reasons to justify the observed high specific capacitance exhibited by the porous Co/MnO@C-700 electrodes were proposed. On one hand, the *in situ* synthetic procedure starting from the crystalline MOF structure is unique in rendering combined fine Co/MnO NPs uniformly supported in the carbon matrix, which prevented the hybrid metal/metal oxides shedding or growing into the larger particles. On the other hand, electrolyte ion diffusion between the active centers (the metal and metal oxide NPs) and efficient electron transfer becomes favored due to the large specific surface area and porosity obtained in the carbon matrix. Electrochemical impedance spectroscopy measurements were carried out with these electrodes show that the semicircle diameter for the Co/MnO@C-700 electrode was the smallest (Figure 13 c), indicating a faster charge transfer rate and lesser resistance compared to the other samples.

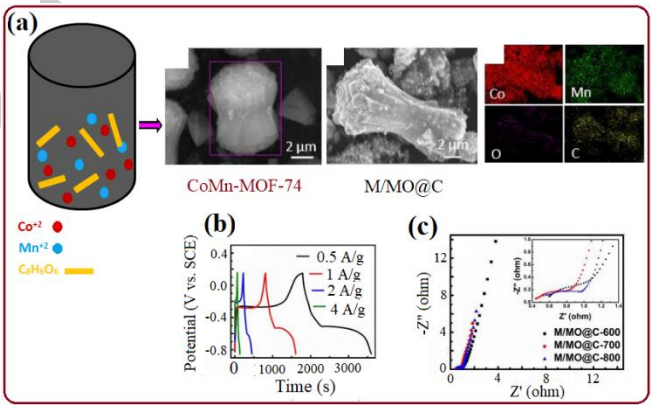


**Figure 13.** (a) Schematic synthesis and characterization of Co/Mn-MOF-74 and Co/MnOx@C samples with SEM images and mapping analysis, (b) GCD curves of Co/MnOx@C-700 electrode material at different current densities, and (c) Electrochemical impedance spectra of Co/MnOx@C samples. Reproduced with permission from Ref.[58] Copyright 2016, the Royal Society of Chemistry..

In a further increase of complexity in MOF transformation, a hybrid MnS/$MoS_2$/C composite was prepared via Mn/Mo-MOF precursor carbonization and subsequent sulfurization (Figure 14 a).[57] In this example, the carbon matrix was again acting as support of the small MnS and $MoS_2$ NPs of the composite and increasing the electrical conductivity and electron transfer rate of the composite. Moreover, a synergistic effect between the MnS

and $MoS_2$ components was also found. The electrochemical response of the MnS/$MoS_2$/microporous C composite was studied in a three-electrode system. Upon cycling, virtually identical symmetric charge-discharge plots were recorded for the MnS/$MoS_2$/C material, demonstrating the high reversibility of the redox cycles in this hybrid material. A decrease in the charging-discharging current density caused a small increase of the charging-discharging time. After 10.000 cycles, the specific capacitance and Coulombic efficiency (˜100 %) of the MnS/$MoS_2$/C composite was outstandingly retained (Figure 14 b). The main reason for this remarkable stability was proposed to be the adequate rate of electrolyte ion distribution and their electrochemical interaction with the active NPs at the electrode interphase over the charging and discharging cycle.[57]

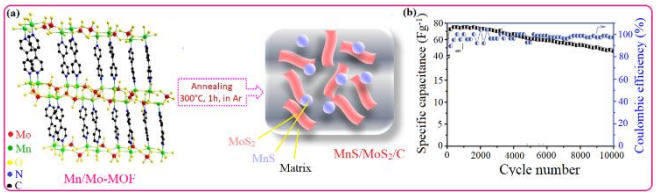


**Figure 14.** (a) Synthesis of MnS/$MoS_2$/C electrode, (b) cyclic stability and Coulombic efficiency of MnS/$MoS_2$/C electrode. Reproduced with permission from Ref.[57] Copyright 2018, The Royal Society of Chemistry.

In a different approach, a two-step method starting from Ni/Co-ZIF-67 was developed by Huang *et al*., who performed sulfurization and subsequent carbon coating to create bimetallic Ni/Co sulfides ($Ni_{3x}Co_{3-3x}S_4$), (NCS) coated by carbon ($Ni_{3x}Co_{3-3x}S_4$@carbon) (NCS@C) hollow dodecahedrons.[55] SEM images revealed a smooth surface with an ordered hollow dodecahedral structure (Figure 15 a). NCS@C-based electrodes demonstrated an improved specific capacitance, charge/discharge rate and cyclic stability compared to bare monometallic CoS and NCS. The carbon coating contributed to the EDLC value, while the NCS contributed with Faradaic redox reactions. This dual contribution displayed in the specific capacitance by the NCS@C-based electrodes has been pointed out as the main reason for its improved electrochemical efficiency.[55]

GCD plots of NCS@C showed a nearly symmetric capacitive activity.[55] Figure 15 b compiles capacitance values as a function of the current density for NCS@C and NCS to show their relative performance. Only a 10.9 % decrease in capacitance was demonstrated for the NCS@C electrode at low current densities (1-5 A $g^{-1}$), while a significantly larger 31.7 % reduction was measured for NCS over similar current densities. As presented in Figure 15 c, the NCS@C electrode capacitance retention over 2000 cycles was of 73 %, while the one for NCS was of 58 %. Among the reasons for the cycling stability, carbon coating has been proposed to be the most important one since it improves the structure mechanical strength, and thus, makes the active components to withstand the electrochemical stress under high current, resulting in an enhancement of the structural integrity.[99]

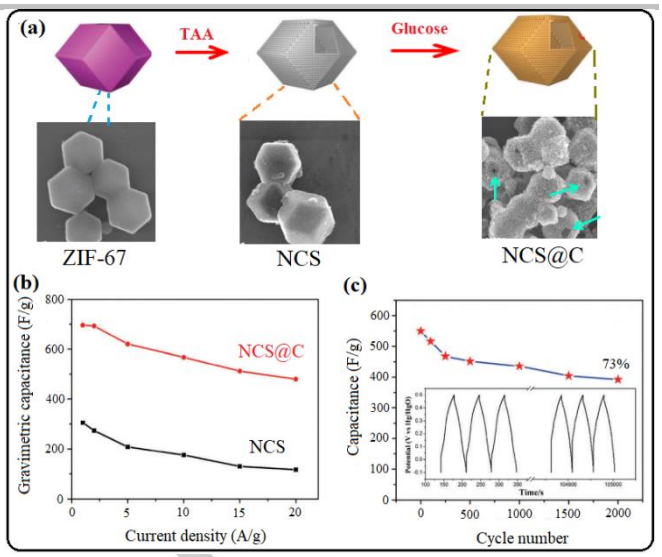


**Figure 15.** (a) Ordered hollow dodecahedral structure of ZIF-67, NCS and NCS@C samples, (b) Gravimetric capacitance of NCS and NCS@C samples versus different current densities, and (c) Cyclic behavior of NCS@C for 2000 cycles. Reproduced with permission from Ref.[55] Copyright 2018, the Royal Society of Chemistry.

An energy density of 7.0 W h $kg^{-1}$ at a power density of 100.4 W $kg^{-1}$ was demonstrated, and an energy density of 4.8 W h $kg^{-1}$ at a power density of 490.0 W $kg^{-1}$ was still maintained by the NCS@C//AC ASD after measurements.[55]

Similarly, Young *et al*. reported the preparation and characterization of $NiCo_2O_4$ nanosheets supported on polyhedral-shaped nanoporous carbon particles (NCP).[63] The NCP were synthesized by zeolitic imidazole frameworks (ZIF-8) carbonization (Figure 16 a), while the $NiCo_2O_4$ nanosheets were subsequently incorporated onto the porous NCP template. The authors reported a pore volume of 0.10 $cm^3$ $g^{-1}$ and 20 $m^2$ $g^{-1}$ surface area for the $NiCo_2O_4$, while the surface area and pore volume values of the $NiCo_2O_4$-NCP composite were of 126 $m^2$ $g^{-1}$ and 0.53 $cm^3$ $g^{-1}$, respectively. Pore size distribution analysis revealed the existence of mesopores with dimensions in the range of 3-10 nm, corresponding to the voids between the individual nanosheets.[63]

In order to assess the electrochemical performance of these samples, a standard three-electrode system was utilized. According to the CV measurements, 157, 40, and 310 F $g^{-1}$ were obtained at 5 mV $s^{-1}$ scan rate in NCP, $NiCo_2O_4$, and $NiCo_2O_4$-NCP samples, respectively (Figure 16 b). The higher capacitance determined in NCP samples over the $NiCo_2O_4$ was attributed to its higher specific surface area (1823 $m^2$ $g^{-1}$).[63] The authors reported that the enhanced capacitance of the $NiCo_2O_4$-NCP nanocomposite was consequence of the synergy effect between the porous NCP framework and the $NiCo_2O_4$ nanosheets. According to this proposal, the porous NCP framework provides an excellent platform for performing electrochemical reactions due to its high surface area and electrical conductivity. $NiCo_2O_4$ nanosheets, on the other hand, conveniently carries out the redox reactions, improving significantly the electrochemical performance of this hybrid composite.[63]

ASD using $NiCo_2O_4$-NCP and NCP as the positive and negative electrodes, respectively, were built and their performance as electrical energy storage devices studied. Nearly no distortion and well-defined redox peaks were observed in the

CV curves providing an optimum 1.5 V working voltage. This ASD delivered also a maximum energy density and power density of 28 W h $kg^{-1}$ and 8.5 kW $kg^{-1}$, respectively, making an optimal use of the extended potential window.[63]

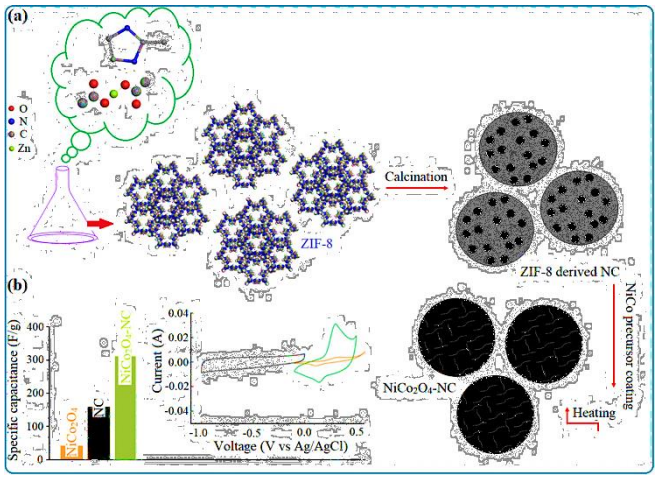


**Figure 16.** (a) Synthesis of a novel $NiCo_2O_4$-NC hybrid material and (b) specific capacitance of $NiCo_2O_4$, NC, and $NiCo_2O_4$-NC electrode materials at a scan rate of 5 mV $s^{-1}$. Reproduced with permission from Ref.[63] Copyright 2017, the Royal Society of Chemistry.

In a different example, a one-pot co-preparation technique was developed by Rahmanifar *et al*. to prepare Ni/Co-MOF-rGO nanocomposites from Co and Ni MOF precursors and reduced graphene oxide (rGO) without the need of high temperature (Figure 17).[64] This nanocomposite showed a specific capacitance of 860 $Fg^{-1}$ at a current density of 1 $Ag^{-1}$. The conductivity of the electrode material, which is an important factor for SCs, was studied by electrochemical impedance spectroscopy. The results confirmed that the capacitive efficiency of the Ni/Co-MOF-rGO nanocomposite was higher than the capacitive efficiency of other materials, a fact that was attributed to the electrical conductivity provided by the rGO. Additionally, for practical application, a two-electrode ASD was prepared to study the Ni/Co-MOF-rGO nanocomposite energy storage capacity. The ASD worked in the potential range from 0 to 1.6 V. This device provided a remarkable specific energy (72.8 W h $kg^{-1}$ at 1 A $g^{-1}$) with a specific power of 850 W $kg^{-1}$, and exhibited a progressed specific power density of up to 42.5 W $kg^{-1}$ at a specific energy density of 15.1 W h $kg^{-1}$ (at a current density of 50 A $g^{-1}$), demonstrating that the aforementioned device allows a great rate of charge-discharge.[64] In other paper, copper-iron 1,3,5-benzene tricarboxylic acid (CuFeBTC)-based bimetallic MOF and its hybrid nanocomposite with S-doped graphene (S-GNS) have synthesized by an easy wet chemical method and have been utilized as supercapacitor electrodes. In, SGNS because of high conductivity, SGNS anchored to the bimetallic MOF NPs in CuFeBTC/S-GNS nanocomposite play a role as current nanocollectors. The unique characteristics of bimetallic MOF and heteroatom doped graphene including tunable porosity, significant specific surface area as well as high electrical conductivity considerably improve the total electrochemical efficiency of this hybrid composite. Specially, great porous and hollow structure of the material provided for the transfer of electrolyte ions due to the great porous and hollow structure of the material. As a result the charge transport across the electrode/electrolyte interfaces is elevated. Furthermore, Electrolyte ions can readily penetrate in the active material owing to the presence of active redox sites in the bimetallic MOF and significant conductivity of S-GNS in the nanocomposite resulting in great specific capacitance. An operational voltage of 1.8 V was obtained for the constructed symmetric supercapacitor where displays an exceptional cycle life of 10,000 cycles and preserves ~92.5% of its initial specific capacitance at a current density of 1.0 A $g^{-1}$. Therefore, above findings indicate that CuFeBTC/S-GNS hybrid nanocomposite can be employed as a useful tool in advanced energy storage systems.[69]

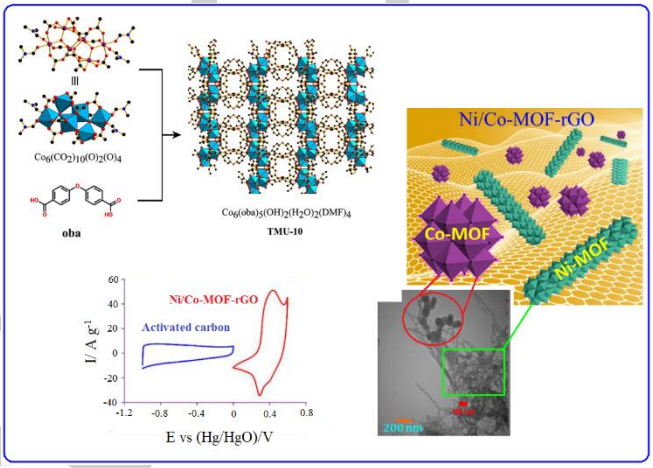


**Figure 17.** Schematic illustration of Ni/Co-MOF-rGO nanocomposite as an electrode material in SCs**.** Reproduced with permission from Ref.[64] Copyright 2018, Elsevier Inc.

As it has been approved by recent investigations, preparation of the composites of carbon encapsulated metal phosphide NPs can increase their stability and rate efficiency in a better way. Electronic conductivity of the composites is enhanced by introducing carbon leading to the fast electron transport. An investigation utilized calcination/phosphorization of MOF precursors to synthesize different $Ni_mP_n$/C, $Ni_2P$/C, $Co_2P$/C and $Ni_xCo_{2-x}P$/C nanohybrids having different Ni/Co molar ratios. The NiCoP/C materials have granular structures and a lot of carbons are anchored to the NiCoP NPs. The most noticeable specific capacities of 775.7C $g^{-1}$ at 1 A $g^{-1}$, and 582.4C $g^{-1}$ at 20 A $g^{-1}$ (20-fold) and the significant rate capability of 75.1% retention was provided by the as-prepared NiCoP/C specimen due to the bimetallic synergism as well as carbon anchoring effect. These values are much higher than those listed for corresponding $Ni_mP_n$/C, $Ni_2P$/C, $Co_2P$/C, other $Ni_xCo_{2-x}P$/C specimens and other different investigated metal phosphide nanostructures/nanocomposites.[70]

## 5. Summary and Outlook

Development of efficient energy storage systems has become a subject of uppermost importance recently. The next generation of electrical energy storage devices, including batteries or SCs, urgently needs novel and highly efficient

materials to satisfy the ever-growing request for higher power and energy densities.

In recent years, MOFs have attracted considerable attention as propitious electrode materials in SCs. Due to the wide range of available organic linkers and metal ions, unlimited MOFs structures can be designed and one of the long-sought target is to synthesis task-specific MOFs whose properties fit for their direct usage in the area of energy storage and conversion, especially in fuel cells, batteries, and SCs. Nevertheless, up to now it has not possible to exploit the potential of MOFs in the area of renewable energy sources since MOFs possess a very limited electrical conductivity.

The issues to be addressed in the future include: i) stability improvement of pristine bimetallic MOFs in electrochemical tests conditions for SCs making the capacitance loss upon the number of charge/discharge cycles closer to industrial requirement, ii) organic electrolytes compatible with pristine MOFs and potential windows higher than the aqueous electrolytes, iii) deposition and adherence of bimetallic MOFs in electrodes and suitable design of SCs, iv) diminish electrical resistance making the specific capacitance of bimetallic MOFs closer to the theoretical values, and v) increase the low volumetric energy density of MOFs and their low packing density.

Until these limitations are overcome by wise tailoring of MOF backbones using a combination of various metals as well as conductive ligands or by diminishing the dimensionality of MOFs from 3D to 2D, an alternative is the transformation of MOFs into derived materials that inherit porosity and creates novel morphologies and composites. For this reason, MOFs are regarded as templates providing spatial structuring and porosity to the derived material. Most of the cases reported so far refer to the use of monometallic MOFs as templates.

The present review has shown the advantages that materials derived from bimetallic MOFs as sacrificial templates to obtain bimetallic oxides, sulfides, hydroxides, and selenides to prepare electrodes for SCs, highlighting the newest and most relevant MOF-derived bimetallic materials. Compared to analogous MOF-derived monometallic materials, higher capacitance values, energy and power density have been achieved using bimetallic materials. The current understanding attributes the improved performance of bimetallic materials as electrodes to the appearance of a synergy caused by the presence of the two metals, increasing electrical conductivity, charge/discharge cycling stability and electron transfer rates. Regarding a more detailed understanding and theory-driven research, it is worth mentioning that the area is lacking of clear computational calculations and modelling on the nature of optimal active sites, operation mechanisms and the bottlenecks limiting reaching higher energy densities. These calculations, after proper experimental validation, should lead the field in the search for the best-performing materials with the appropriate pore dimensions for each electrolyte and with suitable crystal size and morphology.

Given the commercial interest in electrical energy storage, the field is really active with contributions from several disciplines including Chemistry, Materials Science and Energy Engineering. It is expected that the field will progress by this multidisciplinary research, addressing among other the following issues: i) better understanding of the relationship between the composition and material structure with electrode performance, and consequently, the theory-driven selection of bimetallic MOF templates, ii) the design and synthesis of novel bimetallic MOFs that can result in novel structured materials, iii) innovative treatments to convert the MOF into materials with new morphology, higher surface area along with appropriate distribution and size of the pores and high electrical conductivity, iv) compositing materials derived from bimetallic MOFs with other types of materials to accelerate electron transfer, improve structural stability and increases electrolyte access, which could leads to a significant enhancement of the performance of the SC.

Overall, considering that the field is just in its infancy, it can be anticipated that the field will flourish with a whole array of new structured materials based on the properties of MOFs as templates.

## Acknowledgements

This work was supported by Tarbiat Modares University and College of Engineering, Peking University. Financial support by the Spanish Ministry of Science and Innovation (Severo Ochoa and RTI2018-98237-CO2-1) and Generalitat Valenciana (Prometeo 2017-083) is gratefully acknowledged.

**Keywords:** energy storage • supercapacitor • electrode material • MOFs • bimetallic materials

[1] a) K. Solaun, E. Cerdá, *Renewable and Sustainable Energy Reviews* **2019**, *116*, 109415; b) V. V. Quaschning, *Renewable Energy and Climate Change, 2nd Edition*, Wiley, **2019**; c) D. Gielen, F. Boshell, D. Saygin, M. D. Bazilian, N. Wagner, R. Gorini, *Energy Strategy Reviews* **2019**, *24*, 38-50.

[2] a) S. Ould Amrouche, D. Rekioua, T. Rekioua, S. Bacha, *International Journal of Hydrogen Energy* **2016**, *41*, 20914-20927; b) Q. Zhang, E. Uchaker, S. L. Candelaria, G. Cao, *Chemical Society Reviews* **2013**, *42*, 3127-3171.

[3] a) Y. Shao, M. F. El-Kady, J. Sun, Y. Li, Q. Zhang, M. Zhu, H. Wang, B. Dunn, R. B. Kaner, *Chemical Reviews* **2018**, *118*, 9233-9280; b) M. A. Scibioh, B. Viswanathan, *Materials for Supercapacitor Applications*, Elsevier Science, **2020**; c) J. Liu, J. Wang, C. Xu, H. Jiang, C. Li, L. Zhang, J. Lin, Z. X. Shen, *Advanced Science* **2018**, *5*, 1700322.

[4] F. Wang, X. Wu, X. Yuan, Z. Liu, Y. Zhang, L. Fu, Y. Zhu, Q. Zhou, Y. Wu, W. Huang, *Chemical Society Reviews* **2017**, *46*, 6816-6854.

[5] M. Horn, J. MacLeod, M. Liu, J. Webb, N. Motta, *Economic Analysis and Policy* **2019**, *61*, 93-103.

[6] A. K. Samantara, S. Ratha, *Materials development for Active/Passive Components of a Supercapacitor*, Springer, Singapore, **2018**.

[7] A. C. Forse, C. Merlet, J. M. Griffin, C. P. Grey, *Journal of the American Chemical Society* **2016**, *138*, 5731-5744.

[8] a) J. Wu, Q. e. Zhang, J. Wang, X. Huang, H. Bai, *Energy & Environmental Science* **2018**, *11*, 1280-1286; b) C. Zequine, C. K. Ranaweera, Z. Wang, S. Singh, P. Tripathi, O. N. Srivastava, B. K. Gupta, K. Ramasamy, P. K. Kahol, P. R. Dvornic, R. K. Gupta, *Scientific Reports* **2016**, *6*, 31704; c) R. Dubey, V. Guruviah, *Ionics* **2019**, *25*, 1419-1445.

[9] a) C. Costentin, T. R. Porter, J.-M. Savéant, *ACS Applied Materials & Interfaces* **2017**, *9*, 8649-8658; b) B. Viswanathan, in *Energy Sources* (Ed.: B. Viswanathan), Elsevier, Amsterdam, **2017**, pp. 315-328; c) P. Simon, Y. Gogotsi, B. Dunn, *Science* **2014**, *343*, 1210-1211.

[10] a) A. Muzaffar, M. B. Ahamed, K. Deshmukh, J. Thirumalai, *Renewable and Sustainable Energy Reviews* **2019**, *101*, 123-145; b) A. Afif, S. M. H. Rahman, A. Tasfiah Azad, J. Zaini, M. A. Islan, A. K. Azad, *Journal of Energy Storage* **2019**, *25*, 100852.

[11] a) Poonam, K. Sharma, A. Arora, S. K. Tripathi, *Journal of Energy Storage* **2019**, *21*, 801-825; b) J. Sun, C. Wu, X.

Sun, H. Hu, C. Zhi, L. Hou, C. Yuan, *Journal of Materials Chemistry A* **2017**, *5*, 9443-9464.
[12] B. Zhu, D. Xia, R. Zou, *Coordination Chemistry Reviews* **2018**, *376*, 430-448.
[13] a) F. Zhou, H. Huang, C. Xiao, S. Zheng, X. Shi, J. Qin, Q. Fu, X. Bao, X. Feng, K. Müllen, Z.-S. Wu, *Journal of the American Chemical Society* **2018**, *140*, 8198-8205; b) A. Khosrozadeh, G. Singh, Q. Wang, G. Luo, M. Xing, *Journal of Materials Chemistry A* **2018**, *6*, 21064-21077.
[14] a) S. Ortaboy, J. P. Alper, F. Rossi, G. Bertoni, G. Salviati, C. Carraro, R. Maboudian, *Energy & Environmental Science* **2017**, *10*, 1505-1516; b) J. Wei, X. Li, H. Xue, J. Shao, R. Zhu, H. Pang, *Advanced Materials Interfaces* **2018**, *5*, 1701509.
[15] a) W. Tian, Q. Gao, W. Qian, *ACS Sustainable Chemistry & Engineering* **2017**, *5*, 1297-1305; b) X. Wang, C. Yang, J. Jin, X. Li, Q. Cheng, G. Wang, *Journal of Materials Chemistry A* **2018**, *6*, 4432-4442.
[16] a) J. Cao, C. Zhu, Y. Aoki, H. Habazaki, *ACS Sustainable Chemistry & Engineering* **2018**, *6*, 7292-7303; b) H. Dan, K. Tao, Q. Zhou, Y. Gong, J. Lin, *ACS Applied Materials & Interfaces* **2018**, *10*, 31340-31354; c) R. Boddula, M. F. Ahmer, A. M. Asiri, *Morphology Design Paradigms for Supercapacitors*, CRC Press, **2019**.
[17] a) L. Zhu, X.-Q. Liu, H.-L. Jiang, L.-B. Sun, *Chemical Reviews* **2017**, *117*, 8129-8176; b) A. Corma, H. García, F. X. Llabrés i Xamena, *Chemical Reviews* **2010**, *110*, 4606-4655; c) A. Dh..akshinamoorthy, A. M. Asiri, H. Garcia, *Advanced Materials* **2019**, *31*, 1900617; d) Z. Karimi, A. Morsali, *Journal of Materials Chemistry A* **2013**, *1*, 3047-3054; e) P. Z. Moghadam, A. Li, S. B. Wiggin, A. Tao, A. G. P. Maloney, P. A. Wood, S. C. Ward, D. Fairen-Jimenez, *Chemistry of Materials* **2017**, *29*, 2618-2625.
[18] a) R. Abazari, A. Morsali, D. P. Dubal, *Inorganic Chemistry Frontiers* **2020**, *7*, 2287-2304; b) S. Sanati, R. Abazari, A. Morsali, *Chemical Communications* **2020**, *56*, 6652-6655; c) S. S. Shinde, C. H. Lee, J.-Y. Jung, N. K. Wagh, S.-H. Kim, D.-H. Kim, C. Lin, S. U. Lee, J.-H. Lee, *Energy & Environmental Science* **2019**, *12*, 727-738; d) A. Kirchon, L. Feng, H. F. Drake, E. A. Joseph, H.-C. Zhou, *Chemical Society Reviews* **2018**, *47*, 8611-8638; e) R. Abazari, F. Ataei, A. Morsali, A. M. Z. Slawin, C. L. Carpenter-Warren *ACS Applied Materials & Interfaces* **2019**, *11*, 45442-45454; f) R. Abazari, A. R. Mahjoub, S. Molaie, F. Ghaffarifar, E. Ghasemi, A. M. Z. Slawin, C. L. Carpenter-Warren *Ultrasonics Sonochemistry* **2018**, *43*, 248-261; g) R. Abazari, A. R. Mahjoub, F. Ataei, A. Morsali, C. L. Carpenter-Warren, K. Mehdizadeh, A. M. Z. Slawin, *Inorganic Chemistry* **2018**, *57*, 13364-13379.
[19] a) M. Ding, R. W. Flaig, H.-L. Jiang, O. M. Yaghi, *Chemical Society Reviews* **2019**, *48*, 2783-2828; b) V. Kumar, P. Kumar, S. Kumar, D. Singhal, R. Gupta, *Inorganic Chemistry* **2019**, *58*, 10364-10376; c) R. Abazari, S. Sanati, A. Morsali, A. Slawin, C. L. Carpenter-Warren, *ACS Applied Materials & Interfaces* **2019**, *11*, 14759-14773.
[20] R. Abazari, S. Sanati, A. Morsali, A. M. Z. Slawin, C. L. Carpenter-Warren, W. Chen, A. Zheng, *Journal of Materials Chemistry A* **2019**, *7*, 11953-11966.
[21] a) R. R. Salunkhe, Y. V. Kaneti, Y. Yamauchi, *ACS Nano* **2017**, *11*, 5293-5308; b) R. Zhao, Z. Liang, S. Gao, C. Yang, B. Zhu, J. Zhao, C. Qu, R. Zou, Q. Xu, *Angewandte Chemie International Edition* **2019**, *58*, 1975-1979.
[22] Z. Liang, C. Qu, W. Guo, R. Zou, Q. Xu, *Advanced Materials* **2018**, *30*, 1702891.
[23] N. Stock, S. Biswas, *Chemical Reviews* **2012**, *112*, 933-969.
[24] a) M. H. Yap, K. L. Fow, G. Z. Chen, *Green Energy & Environment* **2017**, *2*, 218-245; b) F. Marpaung, M. Kim, J. H. Khan, K. Konstantinov, Y. Yamauchi, M. S. A. Hossain, J. Na, J. Kim, *Chemistry – An Asian Journal* **2019**, *14*, 1331-1343.
[25] J. G. Nguyen, S. M. Cohen, *Journal of the American Chemical Society* **2010**, *132*, 4560-4561.
[26] a) *Nature* **2016**, *538*, 143-143; b) K. Wang, X. Wang, D. Zhang, H. Wang, Z. Wang, M. Zhao, R. Xi, H. Wu, M. Zheng, *CrystEngComm* **2018**, *20*, 6940-6949.
[27] X. Liu, C. Shi, C. Zhai, M. Cheng, Q. Liu, G. Wang, *ACS Applied Materials & Interfaces* **2016**, *8*, 4585-4591.
[28] a) L. Sun, M. G. Campbell, M. Dinca, *Angewandte Chemie International Edition* **2016,** *55*, 3566-3579; b) W. Zhu, C. Zhang, Q. Li, L. Xiong, R. Chen, X. Wan, Z. Wang, W. Chen, Z. Deng, Y. Peng, *Applied Catalysis B: Environmental* **2018**, *238*, 339-345; c) A. J. Clough, J. M. Skelton, C. A. Downes, A. A. dela Rosa, J. W. Yoo, A. Walsh, B. C. Melot, S. C. Marinescu, *Journal of the American Chemical Society* **2017**, *139*, 10863-10867; d) D. Feng, T. Lei, M. R. Lukatskaya, J. Park, Z. Huang, M. Lee, L. Shaw, S. Chen, A. A. Yakovenko, A. Kulkarni, J. Xiao, K. Fredrickson, J. B. Tok, X. Zou, Y. Cui, Z. Bao, *Nature Energy* **2018**, *3*, 30-36; e) D. Sheberla, J. C. Bachman, J. S. Elias, C.-J. Sun, Y. Shao-Horn, M. Dinca, *Nature Materials* **2017**, *16*, 220-224.
[29] a) L. S. Xie, G. Skorupskii, M. Dinca, *Chemical Reviews* **2020**, *120*, 8536-8580; b) W. Zhang, B. Zheng, W. Shi, X. Chen, Z. Xu, S. Li, Y. Robin Chi, Y. Yang, J. Lu, W. Huang, F.Huo, *Advanced Materials* **2018**, *30*, 1800643; c) Y. Wang, L. Feng, W, Fan, K,-Y,Wang, X. Wang, X. Wang, K. Zhang, X. Zhang, F. Dai, D. Sun, H.-C, Zhou, *Journal of the American Chemical Society* **2019**, *141*, 6967-6975; d) B. S. Gelfand, G. K.H. Shimizu, *Dalton Transactions* **2016**, *45*, 3668-3678.
[30] a) C. Qu, Z. Liang, Y. Jiao, B. Zhao, B. Zhu, D. Dang, S. Dai, Y. Chen, R. Zou, M. Liu, *Small* **2018**, *14*, 1800285; b) J. Liu, D. Zhu, C. Guo, A. Vasileff, S.-Z. Qiao, *Advanced Energy Materials* **2017**, *7*, 1700518.
[31] a) L. Liu, Y. Yan, Z. Cai, S. Lin, X. Hu, *Advanced Materials Interfaces* **2018**, *5*, 1701548; b) M.-L. Yue, C.-Y. Yu, H.-H. Duan, B.-L. Yang, X.-X. Meng, Z.-X. Li, *Chemistry – A European Journal* **2018**, *24*, 16160-16169; c) K.-Y. Zou, Y.-C. Liu, Y.-F. Jiang, C.-Y. Yu, M.-L. Yue, Z.-X. Li, *Inorganic Chemistry* **2017**, *56*, 6184-6196.
[32] Y. Pan, Y. Zhao, S. Mu, Y. Wang, C. Jiang, Q. Liu, Q. Fang, M. Xue, S. Qiu, *Journal of Materials Chemistry A* **2017**, *5*, 9544-9552.
[33] a) K. M. Choi, H. M. Jeong, J. H. Park, Y.-B. Zhang, J. K. Kang, O. M. Yaghi, *ACS Nano* **2014**, *8*, 7451-7457; b) J. Liu, C. Wöll, *Chemical Society Reviews* **2017**, *46*, 5730-5770.
[34] a) M. Y. Masoomi, A. Morsali, A. Dhakshinamoorthy, H. Garcia, *Angewandte Chemie International Edition* **2019**, *58*, 15188-15205; b) S. Abednatanzi, P. Gohari Derakhshandeh, H. Depauw, F.-X. Coudert, H. Vrielinck, P. Van Der Voort, K. Leus, *Chemical Society Reviews* **2019**, *48*, 2535-2565.
[35] a) S. Sundriyal, H. Kaur, S. K. Bhardwaj, S. Mishra, K.-H. Kim, A. Deep, *Coordination Chemistry Reviews* **2018**, *369*, 15-38; b) X. Cao, C. Tan, M. Sindoro, H. Zhang, *Chemical Society Reviews* **2017**, *46*, 2660-2677; c) S. Zheng, H. Xue, H. Pang, *Coordination Chemistry Reviews* **2018**, *373*, 2-21; d) C. Wang, Y. V. Kaneti, Y. Bando, J. Lin, C. Liu, J. Li, Y. Yamauchi, *Materials Horizons* **2018**, *5*, 394-407; e) X.-C. Xie, K.-J. Huang, X. Wu, *Journal of Materials Chemistry A* **2018**, *6*, 6754-6771.
[36] W. Chaikittisilp, M. Hu, H. Wang, H.-S. Huang, T. Fujita, K. C. W. Wu, L.-C. Chen, Y. Yamauchi, K. Ariga, *Chemical Communications* **2012**, *48*, 7259-7261.
[37] S. Horike, D. Umeyama, S. Kitagawa, *Accounts of Chemical Research* **2013**, *46*, 2376-2384.
[38] a) X. Xu, W. Shi, P. Li, S. Ye, C. Ye, H. Ye, T. Lu, A. Zheng, J. Zhu, L. Xu, M. Zhong, X. Cao, *Chemistry of Materials* **2017**, *29*, 6058-6065; b) J. Kim, C. Young, J. Lee, Y.-U. Heo, M.-S. Park, M. S. A. Hossain, Y. Yamauchi, J. H. Kim, *Journal of Materials Chemistry A* **2017**, *5*, 15065-15072; c) Z. Liang, C. Qu, D. Xia, R. Zou, Q. Xu, *Angewandte Chemie International Edition* **2018**, *57*, 9604-9633.
[39] a) H. Yi, H. Wang, Y. Jing, T. Peng, X. Wang, *Journal of Power Sources* **2015**, *285*, 281-290; b) B. Liu, H. Shioyama, H. Jiang, X. Zhang, Q. Xu, *Carbon* **2010**, *48*, 456-463.
[40] in *Novel Carbon Materials and Composites*, pp. 137-167.
[41] J. Qian, X. Wang, L. Chai, L.-F. Liang, T.-T. Li, Y. Hu, S. Huang, *Crystal Growth & Design* **2018**, *18*, 2358-2364.

[42] S. Maiti, A. Pramanik, S. Mahanty, *CrystEngComm* **2016**, *18*, 450-461.

[43] A. T. E. Vilian, B. Dinesh, M. Rethinasabapathy, S.-K. Hwang, C.-S. Jin, Y. S. Huh, Y.-K. Han, *Journal of Materials Chemistry A* **2018**, *6*, 14367-14379.

[44] X.-Y. Yu, L. Yu, H. B. Wu, X. W. Lou, *Angewandte Chemie International Edition* **2015**, *54*, 5331-5335.

[45] S. Zhang, D. Li, S. Chen, X. Yang, X. Zhao, Q. Zhao, S. Komarneni, D. Yang, *Journal of Materials Chemistry A* **2017**, *5*, 12453-12461.

[46] S. Zhang, Z. Yang, K. Gong, B. Xu, H. Mei, H. Zhang, J. Zhang, Z. Kang, Y. Yan, D. Sun, *Nanoscale* **2019**, *11*, 9598-9607.

[47] a) R. R. Salunkhe, J. Tang, Y. Kamachi, T. Nakato, J. H. Kim, Y. Yamauchi, *ACS Nano* **2015**, *9*, 6288-6296; b) J. Yang, C. Zheng, P. Xiong, Y. Li, M. Wei, *Journal of Materials Chemistry A* **2014**, *2*, 19005-19010.

[48] Z. Wu, L. Li, J.-m. Yan, X.-b. Zhang, *Advanced Science* **2017**, *4*, 1600382.

[49] S. Chen, M. Xue, Y. Li, Y. Pan, L. Zhu, S. Qiu, *Journal of Materials Chemistry A* **2015**, *3*, 20145-20152.

[50] P. Yang, X. Song, C. Jia, H.-S. Chen, *Journal of Industrial and Engineering Chemistry* **2018**, *62*, 250-257.

[51] G.-C. Li, P.-F. Liu, R. Liu, M. Liu, K. Tao, S.-R. Zhu, M.-K. Wu, F.-Y. Yi, L. Han, *Dalton Transactions* **2016**, *45*, 13311-13316.

[52] K. Tao, X. Han, Q. Cheng, Y. Yang, Z. Yang, Q. Ma, L. Han, *Chemistry – A European Journal* **2018**, *24*, 12584-12591.

[53] P. Zhang, B. Y. Guan, L. Yu, X. W. Lou, *Angewandte Chemie International Edition* **2017**, *56*, 7141-7145.

[54] C. Chen, M.-K. Wu, K. Tao, J.-J. Zhou, Y.-L. Li, X. Han, L. Han, *Dalton Transactions* **2018**, *47*, 5639-5645.

[55] T. Huang, X.-Z. Song, X. Chen, X.-L. Chen, F.-F. Sun, Q.-F. Su, L.-D. Li, Z. Tan, *New Journal of Chemistry* **2018**, *42*, 5128-5134.

[56] G.-C. Li, M. Liu, M.-K. Wu, P.-F. Liu, Z. Zhou, S.-R. Zhu, R. Liu, L. Han, *RSC Advances* **2016**, *6*, 103517-103522.

[57] Z. S. Yan, J. Y. Long, Q. F. Zhou, Y. Gong, J. H. Lin, *Dalton Transactions* **2018**, *47*, 5390-5405.

[58] Y. C. Wang, W. B. Li, L. Zhao, B. Q. Xu, *Physical Chemistry Chemical Physics* **2016**, *18*, 17941-17948.

[59] C. Qu, B. Zhao, Y. Jiao, D. Chen, S. Dai, B. M. deglee, Y. Chen, K. S. Walton, R. Zou, M. Liu, *ACS Energy Letters* **2017**, *2*, 1263-1269.

[60] H. Mei, Y. Mei, S. Zhang, Z. Xiao, B. Xu, H. Zhang, L. Fan, Z. Huang, W. Kang, D. Sun, *Inorganic Chemistry* **2018**, *57*, 10953-10960.

[61] S.-H. Lee, S. Choi, *Materials Letters* **2017**, *207*, 129-132.

[62] W. Gao, D. Chen, H. Quan, R. Zou, W. Wang, X. Luo, L. Guo, *ACS Sustainable Chemistry & Engineering* **2017**, *5*, 4144-4153.

[63] C. Young, R. R. Salunkhe, S. M. Alshehri, T. Ahamad, Z. Huang, J. Henzie, Y. Yamauchi, *Journal of Materials Chemistry A* **2017**, *5*, 11834-11839.

[64] M. S. Rahmanifar, H. Hesari, A. Noori, M. Y. Masoomi, A. Morsali, M. F. Mousavi, *Electrochimica Acta* **2018**, *275*, 76-86.

[65] S. He, Z. Li, J. Wang, P. Wen, J. Gao, L. Ma, Z. Yang, S. Yang, *RSC Advances* **2016**, *6*, 49478-49486.

[66] Q. Wang, F. Gao, B. Xu, F. Cai, F. Zhan, F. Gao, Q. Wang, *Chemical Engineering Journal* **2017**, *327*, 387-396.

[67] Y. Miao, Y. Sui, D. Zhang, J. Qi, F. Wei, Q. Meng, Y. He, Z. Sun, Y. Ren, *Materials Letters* **2019**, *242*, 42-46.

[68] C. Yu, Y. Wang, J. Cui, D. Yu, X. Zhang, X. Shu, J. Zhang, Y. Zhang, R. Vajtai, Pulickel M. Ajayan, Y. Wu, *Journal of Materials Chemistry A* **2018**, *6*, 8396-8404.

[69] A. S. Rajpurohit, N. S. Punde, A. K. Srivastava, *Journal of Colloid and Interface Science* **2019**, *553*, 328-340.

[70] Q. Zhou, Y. Gong, K. Tao, *Electrochimica Acta* **2019**, *320*, 134582.

[71] J. Linnemann, L. Taudien, M. Klose, L. Giebeler, *Journal of Materials Chemistry A* **2017**, *5*, 18420-18428.

[72] a) H.-L. Jiang, B. Liu, Y.-Q. Lan, K. Kuratani, T. Akita, H. Shioyama, F. Zong, Q. Xu, *Journal of the American Chemical Society* **2011**, *133*, 11854-11857; b) J. Y. Cheong, W.-T. Koo, C. Kim, J.-W. Jung, I.-D. Kim, *ACS Applied Materials & Interfaces* **2018**, *10*, 20540-20549; c) L.-L. Wu, Q.-S. Wang, J. Li, Y. Long, Y. Liu, S.-Y. Song, H.-J. Zhang, *Small* **2018**, *14*, 1704035.

[73] A. Dhakshinamoorthy, Z. Li, H. Garcia, *Chemical Society Reviews* **2018**, *47*, 8134-8172.

[74] a) M.-T. Li, N. Kong, Y.-Q. Lan, Z.-M. Su, *Dalton Transactions* **2018**, *47*, 4827-4832; b) S. Zheng, X. Li, B. Yan, Q. Hu, Y. Xu, X. Xiao, H. Xue, H. Pang, *Advanced Energy Materials* **2017**, *7*, 1602733; c) W. Du, Y.-L. Bai, J. Xu, H. Zhao, L. Zhang, X. Li, J. Zhang, *Journal of Power Sources* **2018**, *402*, 281-295; d) J.-J. Zhou, X. Han, K. Tao, Q. Li, Y.-L. Li, C. Chen, L. Han, *Chemical Engineering Journal* **2018**, *354*, 875-884.

[75] a) D. Jung, L. M. A. Saleh, Z. J. Berkson, M. F. El-Kady, J. Y. Hwang, N. Mohamed, A. I. Wixtrom, E. Titarenko, Y. Shao, K. McCarthy, J. Guo, I. B. Martini, S. Kraemer, E. C. Wegener, P. Saint-Cricq, B. Ruehle, R. R. Langeslay, M. Delferro, J. L. Brosmer, C. H. Hendon, M. Gallagher-Jones, J. Rodriguez, K. W. Chapman, J. T. Miller, X. Duan, R. B. Kaner, J. I. Zink, B. F. Chmelka, A. M. Spokoyny, *Nature Materials* **2018**, *17*, 341-348; b) W. H. Low, P. S. Khiew, S. S. Lim, C. W. Siong, E. R. Ezeigwe, *Journal of Alloys and Compounds* **2019**, *775*, 1324-1356.

[76] P. Mahata, D. Sarma, C. Madhu, A. Sundaresen, S. Natarajan, *Dalton Transactions* **2011**, *40*, 1952-1960.

[77] a) R. Ding, X. Li, W. Shi, Q. Xu, X. Han, Y. Zhou, W. Hong, E. Liu, *Journal of Materials Chemistry A* **2017**, *5*, 17822-17827; b) M. V. Reddy, G. V. Subba Rao, B. V. R. Chowdari, *Chemical Reviews* **2013**, *113*, 5364-5457.

[78] a) D. C. Martínez Casillas, M. P. Longinotti, M. M. Bruno, F. Vaca Chávez, R. H. Acosta, H. R. Corti, *The Journal of Physical Chemistry C* **2018**, *122*, 3638-3647; b) M. F. Lagadec, R. Zahn, S. Müller, V. Wood, *Energy & Environmental Science* **2018**, *11*, 3194-3200.

[79] L. Oar-Arteta, T. Wezendonk, X. Sun, F. Kapteijn, J. Gascon, *Materials Chemistry Frontiers* **2017**, *1*, 1709-1745.

[80] a) J. Jiang, Y. Li, J. Liu, X. Huang, C. Yuan, X. W. Lou, *Advanced Materials* **2012**, *24*, 5166-5180; b) C. Yuan, H. B. Wu, Y. Xie, X. W. Lou, *Angewandte Chemie International Edition* **2014**, *53*, 1488-1504; c) C. Yuan, J. Li, L. Hou, X. Zhang, L. Shen, X. W. Lou, *Advanced Functional Materials* **2012**, *22*, 4592-4597.

[81] X. Lu, X. Huang, S. Xie, T. Zhai, C. Wang, P. Zhang, M. Yu, W. Li, C. Liang, Y. Tong, *Journal of Materials Chemistry* **2012**, *22*, 13357-13364.

[82] a) T. Zhu, E. R. Koo, G. W. Ho, *RSC Advances* **2015**, *5*, 1697-1704; b) F. Li, Y. Xing, M. Huang, K. L. Li, T. T. Yu, Y. X. Zhang, D. Losic, *Journal of Materials Chemistry A* **2015**, *3*, 7855-7861.

[83] Z. Dai, X. Zang, J. Yang, C. Sun, W. Si, W. Huang, X. Dong, *ACS Applied Materials & Interfaces* **2015**, *7*, 25396-25401.

[84] a) M. D. Regulacio, Y. Wang, Z. W. Seh, M.-Y. Han, *ACS Applied Nano Materials* **2018**, *1*, 3042-3062; b) X. Zhu, D. Liu, D. Zheng, G. Wang, X. Huang, J. Harris, D. Qu, D. Qu, *Journal of Materials Chemistry A* **2018**, *6*, 13294-13301.

[85] a) Z. Hu, Z. Zhu, F. Cheng, K. Zhang, J. Wang, C. Chen, J. Chen, *Energy & Environmental Science* **2015**, *8*, 1309-1316; b) T. Stephenson, Z. Li, B. Olsen, D. Mitlin, *Energy & Environmental Science* **2014**, *7*, 209-231; c) X.-Y. Yu, L. Yu, X. W. Lou, *Advanced Energy Materials* **2016**, *6*, 1501333.

[86] a) A. M. Elshahawy, X. Li, H. Zhang, Y. Hu, K. H. Ho, C. Guan, J. Wang, *Journal of Materials Chemistry A* **2017**, *5*, 7494-7506; b) S. Tang, B. Zhu, X. Shi, J. Wu, X. Meng, *Advanced Energy Materials* **2017**, *7*, 1601985.

[87] a) B. Y. Guan, L. Yu, X. Wang, S. Song, X. W. Lou, *Advanced Materials* **2017**, *29*, 1605051; b) Y. M. Chen, Z. Li, X. W. Lou, *Angewandte Chemie International Edition* **2015**, *54*, 10521-10524.

[88] a) M. Pramanik, R. R. Salunkhe, M. Imura, Y. Yamauchi, *ACS Applied Materials & Interfaces* **2016**, *8*, 9790-9797; b) C. Mondal, M. Ganguly, P. K. Manna, S. M. Yusuf, T. Pal, *Langmuir* **2013**, *29*, 9179-9187.

[89] a) W. Peng, H. Li, S. Song, *ACS Applied Materials & Interfaces* **2017**, *9*, 5204-5212; b) S. Gao, Y. Sun, F. Lei, L. Liang, J. Liu, W. Bi, B. Pan, Y. Xie, *Angewandte Chemie International Edition* **2014**, *53*, 12789-12793.

[90] a) J. Li, M. Yang, J. Wei, Z. Zhou, *Nanoscale* **2012**, *4*, 4498-4503; b) T. Bhowmik, M. K. Kundu, S. Barman, *ACS Applied Energy Materials* **2018**, *1*, 1200-1209; c) M. Yu, R. Liu, J. Liu, S. Li, Y. Ma, *Small* **2017**, *13*, 1702616.

[91] a) Y. Chen, W. K. Pang, H. Bai, T. Zhou, Y. Liu, S. Li, Z. Guo, *Nano Letters* **2017**, *17*, 429-436; b) Z. Zhao, H. Wu, H. He, X. Xu, Y. Jin, *Advanced Functional Materials* **2014**, *24*, 4698-4705.

[92] X. Sun, G. Wang, H. Sun, F. Lu, M. Yu, J. Lian, *Journal of Power Sources* **2013**, *238*, 150-156.

[93] a) Q. Ke, C. Guan, X. Zhang, M. Zheng, Y.-W. Zhang, Y. Cai, H. Zhang, J. Wang, *Advanced Materials* **2017**, *29*, 1604164; b) H. Pang, X. Li, Q. Zhao, H. Xue, W.-Y. Lai, Z. Hu, W. Huang, *Nano Energy* **2017**, *35*, 138-145; c) Y. Zhao, L. Hu, S. Zhao, L. Wu, *Advanced Functional Materials* **2016**, *26*, 4085-4093.

[94] T. Han, M.-S. Park, J. Kim, J. H. Kim, K. Kim, *Chemical Science* **2016**, *7*, 1791-1796.

[95] N. L. Torad, M. Hu, S. Ishihara, H. Sukegawa, A. A. Belik, M. Imura, K. Ariga, Y. Sakka, Y. Yamauchi, *Small* **2014**, *10*, 2096-2107.

[96] N. L. Torad, M. Hu, Y. Kamachi, K. Takai, M. Imura, M. Naito, Y. Yamauchi, *Chemical Communications* **2013**, *49*, 2521-2523.

[97] a) J. Tang, R. R. Salunkhe, H. Zhang, V. Malgras, T. Ahamad, S. M. Alshehri, N. Kobayashi, S. Tominaka, Y. Ide, J. H. Kim, Y. Yamauchi, *Scientific Reports* **2016**, *6*, 30295; b) B. Liu, H. Shioyama, T. Akita, Q. Xu, *Journal of the American Chemical Society* **2008**, *130*, 5390-5391.

[98] A. Jayakumar, R. P. Antony, R. Wang, J.-M. Lee, *Small* **2017**, *13*, 1603102.

[99] Y. Chen, Y. Hu, J. Shao, Z. Shen, R. Chen, X. Zhang, X. He, Y. Song, X. Xing, *Journal of Power Sources* **2015**, *298*, 130-137.

## Entry for the Table of Contents

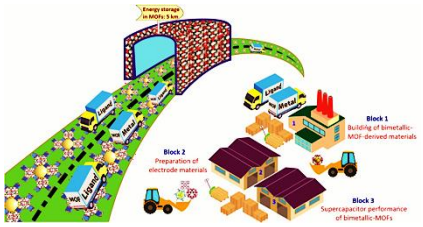


Bimetallic MOFs have been applied as the sacrificial templates or precursors to prepare many different derivatives that can be used in supercapacitors. Bimetallic MOFs and their derivatives can offer advantages of improved electrochemical activity, convenient redox reactions and high electrical conductivity, being very good candidates as advanced electrode materials in this field.